Macromolecules

Perspective

Cite This: Macromolecules 2018, 51, 3−24

Advances in Atomic Force Microscopy for Probing Polymer Structure and Properties

Dong Wang*[,†] and Thomas P. Russell[‡,§,∥]

[†]State Key Laboratory of Organic−Inorganic Composites, College of Materials Science and Engineering, and [‡]Beijing Advanced Innovation Center for Soft Matter Science and Engineering, Beijing University of Chemical Technology, Beijing 100029, China

[§]Polymer Science and Engineering Department, University of Massachusetts Amherst, Amherst, Massachusetts 01003, United States

[∥]Materials Sciences Division, Lawrence Berkeley National Laboratory, 1 Cyclotron Road, Berkeley, California 94720, United States

ABSTRACT: Over the past 30 years, atomic force microscopy (AFM) has played an important role in elucidating the structure and properties of polymer surfaces. AFM-based techniques have enabled the quantitative determination of the physicochemical properties of polymer surfaces with high spatial resolution and under a wide variety of conditions. Coupled with the improvements in spatial and temporal resolution, multiparametric and multifunctional characterization has revealed the delicate interplay between structure, dynamics, and properties at the surfaces of complex systems. Here we summarize some of the significant advances that have been made in synthetic polymeric materials, most in the past 10 years, where AFM has been crucial, and we provide our perspective on where AFM will be insightful in future and instrumental in advancing emerging areas.

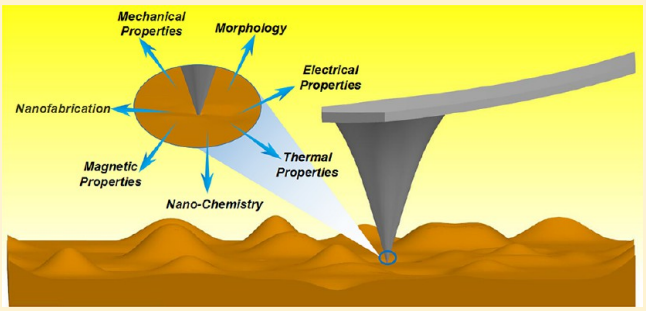

INTRODUCTION

Atomic force microscopy (AFM), since its invention in 1986,[1] has emerged as the dominant tool for imaging the surface topography and quantitatively measuring/mapping the physicochemical properties of a wide range of materials.[2−4] Unlike most imaging techniques that rely on the interaction of photons or electrons with matter, AFM scans a sharp tip attached to the end of a force-sensing cantilever over the surface, measuring the spatial variations of the interactions between the tip and the surface, providing a nanometer-scale (and in some cases atomic-scale) 2D mapping of the mechanical, electrical, magnetic, or topographical properties of the surface.[1−5] The operation conditions of the AFM are flexible, from vacuum to air to liquid media at reduced or elevated temperatures. The AFM tip can also be used for nanomanipulation and nanofabrication.[6] The multiparametric and multifunctional characterization, high spatial resolution, and the wide range of operational conditions have made AFM an exceptionally versatile tool that has given rise to numerous discoveries and technologies and opened new opportunities in physics, chemistry, materials, and biology.[7,8]

Polymeric materials exhibit spatial and temporal heterogeneities in their properties and, for multicomponent systems, chemical composition that fluctuate about an average value. With the rapid development of advanced polymerization techniques,[9−11] polymer morphologies are becoming increasingly more complex. Both the applications and developments pose challenges regarding their micro- and nanoscale structure and properties and how they are coupled and finally lead to the emergent bulk properties that determine their ultimate applications. Consequently, imaging polymeric materials with nanoscale resolution and characterizing the surface morphology and topography, while simultaneously measuring and mapping properties, like the storage and loss modulus, provides a unique means of linking structure to properties, deciphering their relationship, and opening pathways for the development of more advanced materials.

Various microscopy techniques, including AFM, optical microscopy (OM), scanning electron microscopy (SEM), transmission electron microscopy (TEM), transmission electron microtomography (TEMT), laser scanning confocal microscopy (LSCM), and X-ray tomography, have been widely used to study the morphologies of polymeric materials. Among these, generally speaking, only AFM can measure a range of properties of polymeric materials, in addition to providing an image. New imaging modes, such as high-speed (HS) scanning,[12] infrared spectroscopy,[13,14] and multifrequency imaging,[5] have emerged, significantly expanding the spatial and temporal resolution and capabilities of AFM. High spatial and temporal resolution over large areas allows two- or three-dimensional mapping of the surface topography and the variation in properties with sub-nanometer lateral and sub-tenth nanometer height resolution. HS-AFM can record images at a rate of ∼33 frames/s[15] over areas having dimensions from tens of nm to ∼100 μm. Operating conditions can be varied from vacuum to air to liquid media over temperature ranges from

Received: July 10, 2017
Revised: September 21, 2017
Published: October 19, 2017

DOI: 10.1021/acs.macromol.7b01459
Macromolecules 2018, 51, 3−24

subambient to elevated temperatures. Multiparametric images of the structure as well as mechanical (such as adhesion, elasticity, and dissipation), electrical, magnetic, and thermal properties can be measured at the speed of conventional topographic imaging. Nondestructive, time-resolved real-space imaging of dynamics and dynamic processes over length scales from the nanometer to many hundreds of micrometers are readily accessible.

Among a wide variety of AFM modes, amplitude-modulation AFM (usually known as tapping mode AFM), force modes (e.g., single-molecule force spectroscopy, nanoindentation, and AFM nanomechanical mapping), electrical modes (e.g., conductive AFM, photoconductive AFM, and Kelvin probe force microscopy) are commonly used to probe polymeric materials. Moreover, the never-ending developments in the modes of operation strengthen AFM continuously, making it an important, if not indispensible, tool for the characterization of polymeric materials. There have been many reviews and treatises on these different methods[2−4,16−20] and many reviews and books that describe the use of AFM to characterize soft materials;[3,4,21] most though focus on biological systems.[8,22,23]

For all AFM modes, a thorough and fundamental understanding of the tip−sample interaction is needed to obtain high-precision images and reliable data. Even for topography imaging, one must understand that AFM is not a camera or a simple profilometer. For example, the most commonly used tapping mode has two tip−sample interaction regimes: attractive and repulsive.[24,25] The attractive interaction regime allows imaging of the basic morphologies of the sample. More importantly, this regime is able to resolve the detailed structure with high resolution. Imaging in the repulsive interaction regime is associated with the irreversible deformation of a compliant sample, which will lead to a significant loss in resolution and contrast. The crossover between attractive and repulsive regimes will cause changes in height and phase contrast, sometimes appearing as artifacts, and can be related to the particular tip−sample interactions dominating in different set point regimes.[26] Here, it also indicates the "height" images obtained in both regimes, particularly in repulsive regimes, do not necessarily reflect the "real" surface topography of the compliant sample because of sample deformation.[26,27] On the other hand, quantitative nanomechanical mapping has been widely used to measure the nanoscale mechanical properties of polymer materials, but we are still challenged to obtain more than relative values. The factors that affect the accurate measurements of the mechanical properties include not only the commonly stated caveats about unknown tip geometry, errors in instrument calibration (e.g., the cantilever spring constant), or the presence of extrinsic mechanical heterogeneities (e.g., the rigid substrate effect) but also, more importantly, the physical justifications of contact mechanics models on complex polymeric materials.[28−32] Therefore, developing an understanding of the tip−sample interaction and modeling are always essential to achieve and interpret high-quality AFM data (e.g., images, force−distance curves, etc.) and to extract mechanical, electrical, and magnetic properties accurately.

With the rapid development of various AFM techniques, it has now become a routine and, in some cases, an indispensable tool for unravelling the structural and properties of polymers. This is a very broad topic, and as such, we refrain from discussing the wealth of AFM instruments and developments and the basic principles of imaging and measurements in detail here, as they are described in detail in the references cited (e.g., refs 3, 4, 8, and 20). Here, we summarize some of the significant advances that have been made in synthetic polymers, most in the past 10 years, where the advances in AFM played a critical role, and provide some glimpse into future and emerging areas.

STRUCTURE BY AFM: FROM SURFACE MORPHOLOGY TO DYNAMICS

Tapping mode is currently the most commonly used AFM mode for probing polymeric structures. In this mode, the height image depicts the topography, while the phase image, a measure of the energy dissipation during the tip−sample interactions,[33−36] contains information on the elastic, viscoelastic, and adhesive properties of the sample and topography. Tapping mode AFM has been the mainstay for imaging surface topography, characterizing lateral variation in composition, and lateral heterogeneities in dynamics for a wide range of polymers, from glasses to semicrystalline to block copolymers, rubbers, gels, polymer fibers, polymer blends, and polymer composites.[3,4,37]

Surface Mobility and Heterogeneity in Glassy Polymer Thin Films. Thin polymer films have striking dynamic properties that differ from their bulk counterparts and, therefore, have practical implications for thin film coatings, lubrication, adhesion, and friction.[38] There have been substantial efforts to determine the glass transition and dynamics in films, less than ∼100 nm in thickness, using, for example, ellipsometry,[39] dielectric spectroscopy,[40] and X-ray photon correlation spectroscopy (XPCS).[41] Advances in AFM have afforded unprecedented spatial resolution, both parallel to and normal to the film surface, in characterizing the surface topography and viscoelastic properties, providing a direct measure of surface mobility.[42−49]

A fundamental question with thin polymer films is whether there is a reduction in glass transition temperature T_g at the surface and/or if there is a liquid-like layer at the surface. Initial AFM force modulation and lateral force microscopy measurements indicated that the surface mobility of polystyrene (PS) films (200 nm thick) supported on a substrate was higher than that in the bulk, suggesting a reduced T_g at the surface.[42,50,51] An increase in the surface mobility can be explained by an excess free volume arising from chain end localization at the surface,[42,50−52] a reduced cooperativity of segmental motions due to the interface with air or vacuum,[42,50−53] or a looser entanglement of surface chains.[54,55] By capturing very small changes in the surface topography of thin PS films with thermal annealing and analysis of the resultant power spectral density (PSD) data, recent AFM measurements suggested a lower viscosity of surface layer in comparison to the bulk.[46,56] AFM measurements of the surface relaxation using nanoholes (shown in Figure 1a−c)[44] or embedded nanospheres[45,57,58] at the surface of glassy films indicated that the surface relaxed much more rapidly than the bulk and that the surface relaxation had a weaker temperature dependence in comparison to the bulk. Both the reduction of viscosity and the "two-step" embedding process can be explained by a two-layer model, where there is a thin mobile layer with a thickness of a few nanometers.[46,57] The relaxation of artificially made steps in PS was measured above and below T_g by AFM, as shown in Figure 1d−g. The planarization of the film surface above T_g was explained by a flow of the entire film, while below T_g only the thin layer near the free surface could flow.[48] Again, these results are

DOI: 10.1021/acs.macromol.7b01459
Macromolecules 2018, 51, 3−24

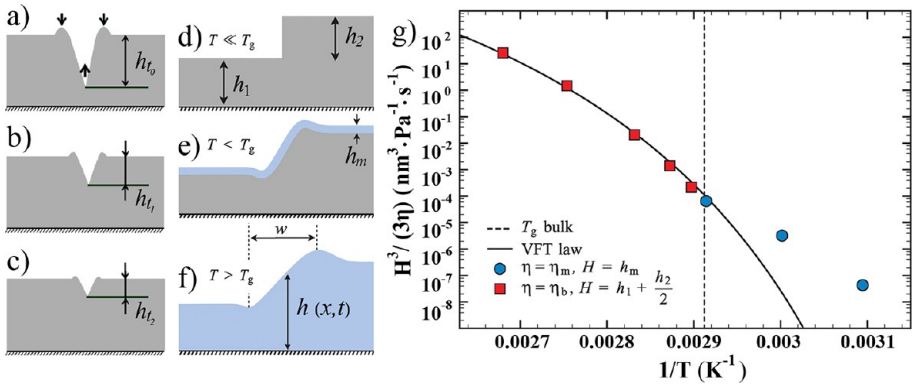

Figure 1. Schematic diagram of the evolution of nanoholes (a–c) and artificially made steps and flow regions (d–f). (a) The height profile of the sample with a nanohole just prepared. The evolution of the depth of the nanohole after annealing times of (b) t_1 and (c) t_2 ($t_1 < t_2$) at a temperature below T_g of the bulk. The depth of the nanohole decreased with the annealing time owing to the surface relaxation. (d) As-prepared sample at room temperature. (e) The evolution of the total height profile $h(x,t)$ through flow localized in a small region near the free surface, corresponding to the flow mechanism at below T_g, and (f) the evolution of the $h(x,t)$ through whole-film flow, corresponding to the flow mechanism at above T_g. The flow region is indicated in blue. (g) Temperature dependence of the surface mobility ($H^3/(3\eta)$). Reproduced with permission from ref 48. Copyright 2014 AAAS.

qualitatively consistent with enhanced mobility at the free surface of polymer thin films. AFM measurements on the relaxation of thin films showed that substrate interactions can also influence the surface mobility.[58,59] Contrary to these observations, however, shear-modulated AFM measurements of surface mobility (at 1400 Hz) of PS thin films were found to be independent of film thickness (17–500 nm), strength of substrate interactions, or even the presence of substrate.[60] This observation may be related to the temperature dependence of surface mobility, where enhancements may be apparent near and below the bulk T_g and, thus, are observable only on very long time scales or at very low frequencies. Measurements performed at higher frequencies, such as those described above, may not be able to discern distinct surface and bulk relaxation processes.[38]

Thermally driven collective dynamics are important for many macroscopic properties of polymers.[61−64] However, our understanding of these dynamics, which are cooperative and heterogeneous, remains limited.[65,66] AFM measurements on the dielectric properties of poly(vinyl acetate) (PVAc) revealed a molecular cooperativity that took the form of transient molecular clusters and nonexponential kinetics near the glass transition.[67] The wide distribution of relaxation times and the strongly nonexponential behavior, which correlates with a broad distribution of spatial fluctuations or structural heterogeneities near T_g, will be frozen-in at T_g and retained in the glassy state. High-resolution AFM[47] and nanomechanical mapping[68] on the surface mechanical properties of PS thin films at room temperature clearly demonstrated nanoscale viscoelastic heterogeneities (shown in Figure 2), 2–3 nm in size, consistent with the size of cooperatively rearranging regions (CRRs) proposed by Adam and Gibbs[69] and as determined by differential scanning calorimetry,[70] and with a variation of 57%.[47,71] The broadly distributed viscoelastic heterogeneities observed in the energy dissipation map suggest there is a wide distribution of energy barriers for configurational rearrangements and structural relaxations at the glass transition. This corresponds to a very broad range of relaxation times and strongly nonexponential behavior as seen in mechanical or dielectric relaxation spectra.[47] The AFM results provide direct experimental evidence for the nanoscale heterogeneities in glassy polymers and provide insights for understanding the origins of the glass transition.

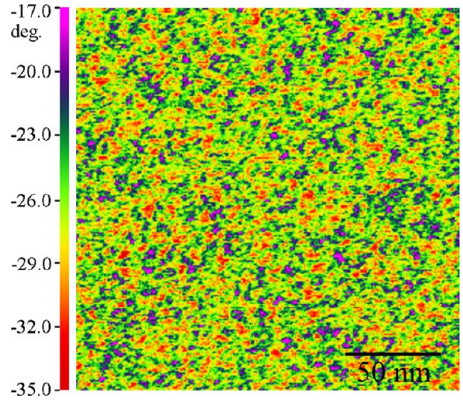

Figure 2. Tapping mode phase image of PS film with ~200 nm thickness. The observed heterogeneity was identified to arise from the inhomogeneous distribution of viscoelastic property. Reproduced with permission from ref 47. Copyright 2012 American Institute of Physics.

Polymer Crystallization. Polymer crystallization is one of the most important topics in polymer science. However, despite more than 60 years of intense study, the way in which polymers crystallize and the fundamental processes, such as the formation of initial nuclei and the growth kinetics resulting in folded intermediate metastable states, which result in their highly complex hierarchical structures, are far from being fully understood.[72] When coupled with a hot stage, AFM is a unique tool for the *in situ* real-time investigation of crystal growth, melting, and reordering process[73−76] at a lamellar and even molecular scale and has provided new insights that could not straightforwardly be obtained with other methods. We focus on the initial development of lamellae and subsequent growth and high-resolution imaging of the crystals. Recent reviews and books[72,77,78] have dealt with many other topics, including oriented crystallization, effects of confinement, the influence of the substrate on crystallization, and the nucleation process.

In situ real-time AFM studies have provided truly unique insights into the growth of lamellae. Studies on melt crystallization of poly(ε-caprolactone) (PCL)[79] and polypropylene (PP)[80] indicate that spiral growths generate additional

DOI: 10.1021/acs.macromol.7b01459
Macromolecules 2018, 51, 3–24

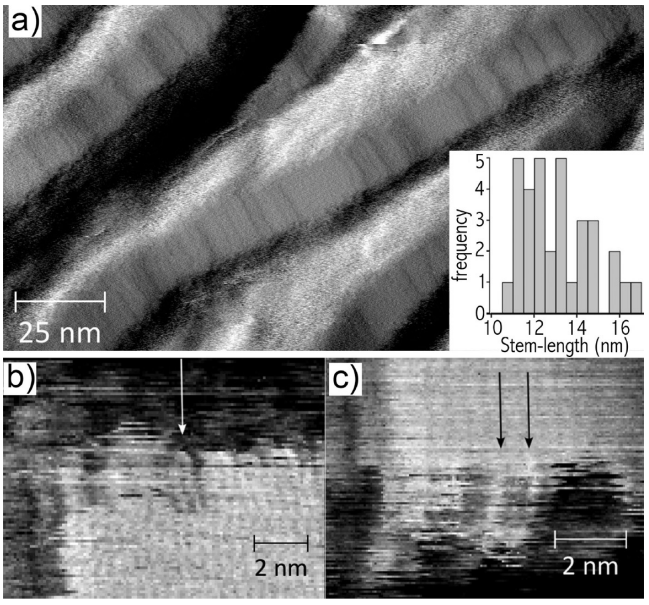

Figure 3. Torsional-tapping AFM images of the oriented "shish-kebab" crystallization of polyethylene. (a) The amplitude image (grayscale 17 mV) clearly visualized molecular steps from which the stems' orientation could be inferred. (Inset) Distribution of widths of lamellae measured along the stem direction. (b) Details from phase images showing a first-neighbor fold, marked by an arrow, and (c) a second-neighbor fold, with arrows marking the two stems. The grayscales represent a phase lag of (b) 7.7° and (c) 9.2°. Reproduced with permission from ref 98.

lamellar layers at low undercoolings. For poly(bisphenol A octane ether) (PBA-C8) an induced nucleation and subsequent branching was found.[81] The growth tip of PBA-C8 was observed to be softer than the rest of the crystal,[82] indicating there may exist intermediate degrees of order that are metastable. Lamellae crystallized from the melt showed a nodular texture,[83,84] suggesting a substructure forms at the growth front of the lamellae, in keeping with the arguments made by Strobl.[85−87] The crystallization rate, as evidenced by the work on individual lamellae and lamellar aggregates, varies from crystal to crystal and for each crystal with time.[72,74]

For spherulite growth, a depletion zone at the front of a growing spherulite was observed.[74,75] Initial crystal growth is followed by a protracted period of a backfilling growth and possibly crystal reorganization.[72] *In situ* observations showed lamellae twisting to produce banded spherulites where the twisting was a continuous over a substantial fraction of the rotation.[88] This observation is consistent with X-ray studies[89] and provides evidence for models on the long distance self-organization of the lamellae.[90,91] Screw dislocation branches[76] and other branching mechanisms[82] were directly visualized. Based on these studies, the formation of a screw dislocation from a defect or fluctuation at the edge of a growing lamella was argued to be the main source of branching in polymers.[72] *Ex situ* AFM observations of polyethylene (PE) crystal growth suggested an instability-driven branching mechanisms, arising from a self-induced pressure gradient due to the difference in densities of the crystalline and amorphous phases.[92,93]

While there are numerous models to describe crystallization, crystallization was not understood on a molecular level. Recently, direct imaging with submolecular resolution, i.e., high-resolution imaging of a two-dimensional (2D) crystal prepared by very slow compression of an isotactic poly(methyl methacrylate) (*i*-PMMA) Langmuir film has been available.[94] The AFM images clearly showed the folding and tie-chains and provided a remarkable snapshot of the arrangement of chains within a crystal.[94] The crystalline nuclei preferentially form at the end of the chains, and the size of the nuclei was found to be independent of the chain length (molecular weight). At extremely slow compression rates, crystallization was promoted, leading to the crystallization of the entire chain.[95] The melting behavior of the 2D *i*-PMMA crystals was also observed *in situ* at high temperatures with molecular resolution.[96] The T_m of the 2D crystals was depressed significantly, by up to 90 °C, and showed a strong dependence on the molecular weight and nature of the substrate. The large depressions in T_m of the 2D crystals could not be explained by a simple modified Thompson−Gibbs equation, creating a theoretical challenge of the age-old problem. The molecular scale observation of 2D

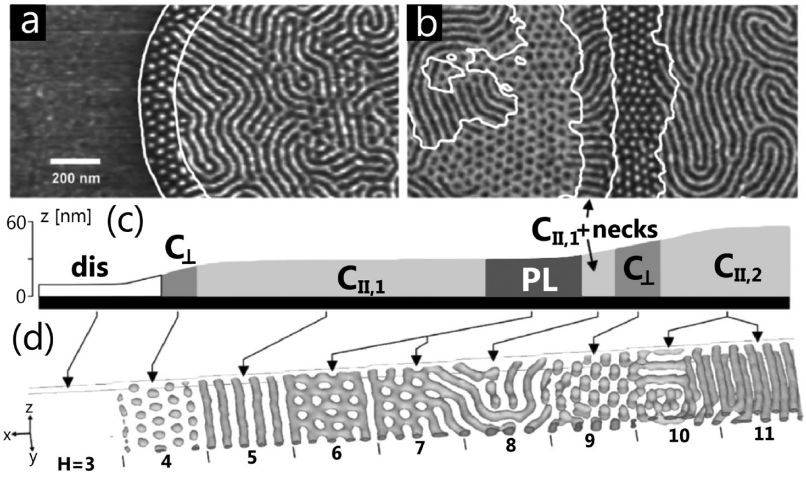

Figure 4. (a, b) Phase images of thin SBS films after annealing in chloroform vapor. Bright (dark) corresponds to PS (PB) microdomains. Contour lines from the corresponding height images are superimposed. (c) Schematic height profile of (a) and (b). (d) Simulated morphology of a BCP film in one large simulation box with increasing film thickness (from left to right). Reproduced with permission from ref 105. Copyright 2002 American Physical Society.

DOI: 10.1021/acs.macromol.7b01459
Macromolecules 2018, 51, 3−24

crystals has provided new insights into the polymer crystallization and has presented new challenges.

Direct imaging of chains within a three-dimensional semicrystalline material has been done (Figure 3).[97,98] Torsional tapping mode AFM imaging of PE, with a 0.37 nm resolution, showed individual chains in the crystalline lattice in air under ambient conditions.[97] Loose molecular loops at the crystal−amorphous interface and the existence of a tight adjacent fold within this interfacial region were observed.[97] Images of this nature have put to rest the very long-standing debate of the adjacent re-entry or random switchboard models.[99,100] Results from such studies can be directly compared to polymer crystallization theories and molecular simulations, addressing very detailed issues, like the length of stem-to-stem overhang, as shown in Figure 3a.[98]

High-resolution AFM imaging has provided insight into almost every aspect of polymer science and has mapped nanoscale mechanical heterogeneities in glassy polymers[47] and has been used to characterize phase separation in polymer-based bulk heterojunction (BHJ) organic photovoltaics (OPV).[101] Because of structural similarities and low imaging contrast between polymer donors and fullerene acceptors, visualizing structure can be difficult.[102] High-resolution AFM imaging of PTB7/PCBM active layers showed the free surface was enriched with polymer crystals having a "face-on" orientation and an average spacing of ∼1.9 nm, and the morphology at the anode interface was markedly different.[101]

Block Copolymer Assembly. AFM has been extensively used to study block copolymer (BCP) self-assembly,[103−105] which has recently attracted significant interest from both industry and academia, since the resultant bulk and thin film morphologies offer ideal platforms for the generation of nanoscopically ordered patterns for a range of promising applications.[106−109] Therefore, an in-depth understanding of these ordered nanostructures with material characteristics and film preparation conditions is essential to further tailor the synthesis of BCPs and for the fabrication of nanopatterns or arrays (Figure 4). In most cases, AFM is combined with electron microscopies or X-ray-based scattering methods to reveal the effects of composition, molecular weight, interaction parameter, interfacial interactions, film thickness, annealing, crystallization, additives, and chain rigidity on the assembly process and the resultant size, shape, and orientation of these nanoscopic structures.[107,109] Correct assignment of the observed surface pattern to a particular morphology is important for the interpretation of the morphological behavior in thin films. Beyond routine applications, however, advances in AFM make it ideal for studying structural defects and dynamics, self-assembly process, where the aggregates are swollen or filled with solvent (such as micelles or vesicles), and changes of the shape due to deposition on the solid surface and drying.

Structural defects in BCP thin films are common and are known to compromise the long-range lateral order that limit the technological performance of BCPs.[107,110−113] AFM studies on BCP thin films have identified classical defects (i.e., disclinations and dislocations) as well as grain boundary defect configurations.[110,112−115] It was found that the motion of lateral defects in cylinder-forming BCPs was diffusion controlled.[114] The minimum feature spacing accessible in thin films is limited by thermal defect generation, not by the bulk order−disorder temperature (ODT).[116] Such defect densities and the ODT are highly sensitive to variations as small as 2 nm in the microdomain spacing.[116] The large shift of monolayer and bilayer ODT caused by variations of the monolayer domain spacing can be explained by the energetic cost of defect production in terms of the domain spacing, interaction parameter, and BCP composition.[116] Early works using time-resolved AFM identified relinking, joining, and clustering as basic processes of structural rearrangements.[112] When applying an electric field to ABC BCP thin films, AFM showed two distinct defect types that govern the orientation mechanism.[117] Moreover, *in situ* imaging of the dynamics and defect annihilation of polystyrene-*b*-polybutadiene-*b*-polystyrene (SBS) during solvent annealing showed a low interfacial energy difference between the cylinder and perforated lamella phases that may account for the energetically favorable path way of structural rearrangements by temporal phase transitions,[118,119] which was also observed by *in situ* AFM imaging of SB diblock copolymers under thermal annealing.[111] This structural rearrangement consists of several elementary dynamic processes, such as short-term interfacial undulations, fast repetitive transitions between distinct defect configurations,[120] and collective/coordinated movement of annihilating defects,[114,120] as revealed by high-speed AFM scanning. The fast dynamics of individual defects and their annihilation in thin films of a cylinder-forming BCPs[121] are illustrated in Figure 5.

BCP micelles, vesicles, and other aggregate structures have emerged as versatile drug delivery systems, nanoreactors, or as templates for nanoparticle synthesis.[122,123] Besides scattering-based methods[124] and wet scanning and cryogenic TEM,[125] AFM has been used to provide *in situ* information about the growth of these aggregate structures in solution by tracking the shape of self-assembled aggregates.[126−128] Varying the architecture of the BCPs, the nature of the solution,[126,127] and the underlying surface[126,128] have opened numerous routes to control surface topology, domain size, and wall thickness of the aggregate structures. For example, the poly(2-(dimethylamino)ethyl methacrylate)-*b*-poly(methyl methacrylate) (DMA-MMA) adsorbed on mica showed surface micelles at low pH and regions of close-packed structure at higher pH, indicating the importance of pH in the resultant morphology of

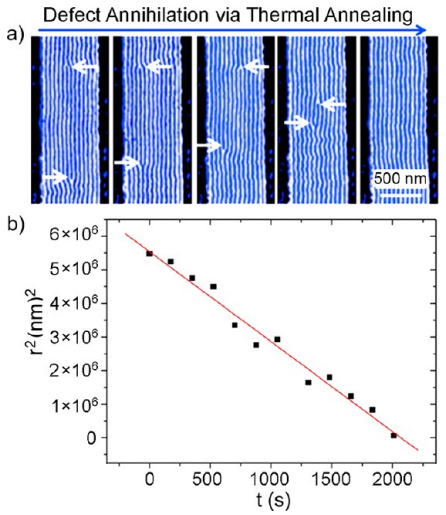

Figure 5. (a) AFM phase images visualized climb motion of two dislocations of opposite Burgers vectors with annealing time. The two dislocation cores were indicated by the arrows. (b) The plot of square of the distance between the two dislocation cores versus corresponding time. Reproduced with permission from ref 121.

DOI: 10.1021/acs.macromol.7b01459
Macromolecules 2018, 51, 3−24

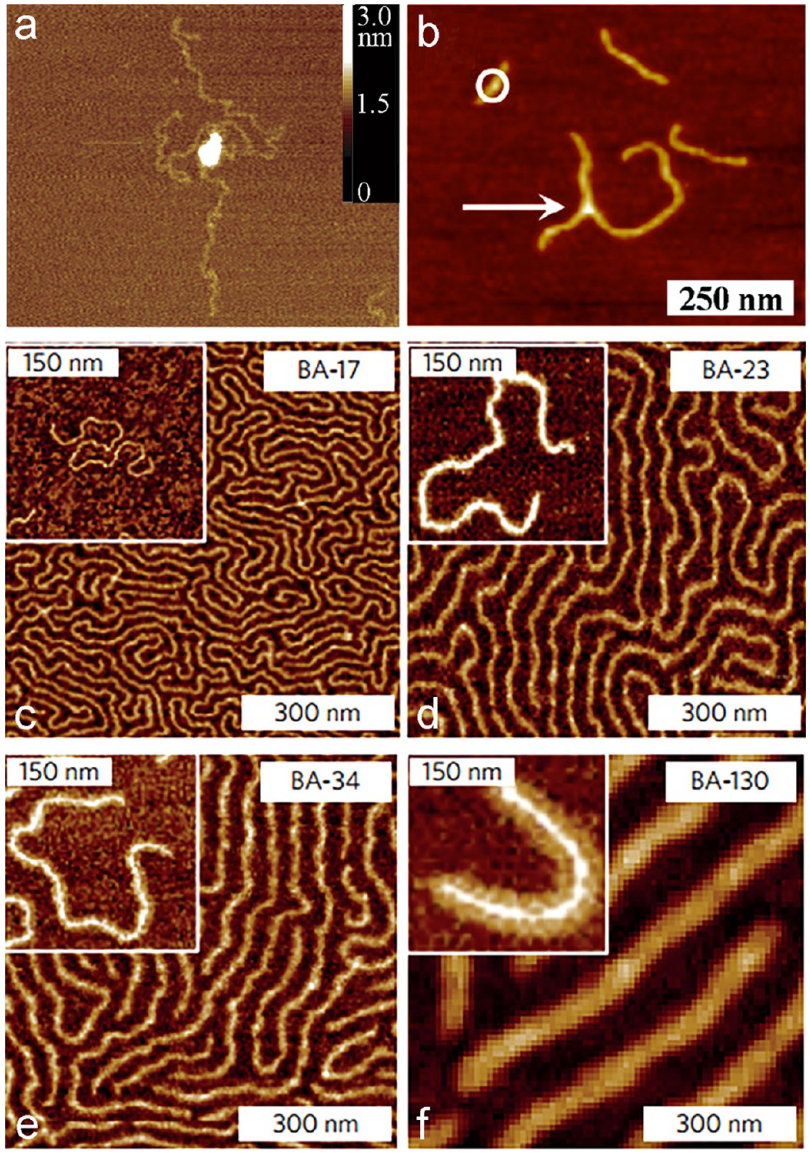

Figure 6. (a) AFM height image of polystyrene-*b*-poly(methyl methacrylate) (PS-*b*-PMMA). The width scale of (a) is 500 nm. Reproduced with permission from ref 169. (b) AFM image of poly(*n*-butyl acrylate) (PBA) brushes made from poly(alkyl acrylate) and poly(alkyl methacrylate) backbones (white arrow pointing to branch junctions). Reproduced with permission from ref 174. (c) AFM height images of the PBA bottlebrushes with the same backbone but different of the degree of polymerization of side chains on a mica substrate. Large images: LB monolayers. Insets: single molecules prepared by spin-casting. Reproduced with permission from ref 170. Copyright 2016 the Nature Publishing Group.

the polyelectrolyte diblock.[126,128] For a poly(oyxethylene)-*b*-poly(oxypropylene) diblock, a more highly ordered structure was found on a hydrophobic silica substrate,[128] demonstrating the importance of the chemical nature of the surface on the resultant morphology of the amphiphilic diblock.

Polymer Subsurface Structure. The surface and bulk morphologies of polymeric systems are often different. Reconstruction of three-dimensional (3D) structures is becoming increasingly important.[129] TEMT has been widely used to this end.[130] AFM is a surface technique, but if sectioning or etching is used in tandem with AFM, subsurface structures can be determined. This was demonstrated in the elucidation of the bicontinuous interpenetrating network in PTB7-based bulk heterojunction active layers.[101,131] Nano-tomography[132] has also been developed for the *in situ* observation of crystal growth of elastomeric polypropylene, where the origins of a lamellar branch was found to originate in a screw dislocation.[133] This layer-by-layer imaging technique was further developed to operate under various conditions and AFM modes[134−136] and found use in the solvent vapor annealing of BCPs under electric fields[137] and visualization of conductive 3D networks of polymer/MWCNT nanocomposites using c-AFM.[135]

The methods described above involve destructive sectioning or etching procedures. Nondestructive subsurface structure imaging by AFM is under very active development with some progress being made using ultrasonic wave or energy dissipation. These have been demonstrated in several polymeric and cellular systems.[138−141] For example, the reconstruction of the subsurface structure of supramolecular aggregates of oligothiophenes yielded a 3D picture consisting of 15 nm wide fibrils with a rigid core and a soft shell.[140] In the P3HT system, the crystalline regions and crystalline fibers were found to be covered by an ∼7 nm amorphous layer after solvent

DOI: 10.1021/acs.macromol.7b01459
Macromolecules 2018, 51, 3−24

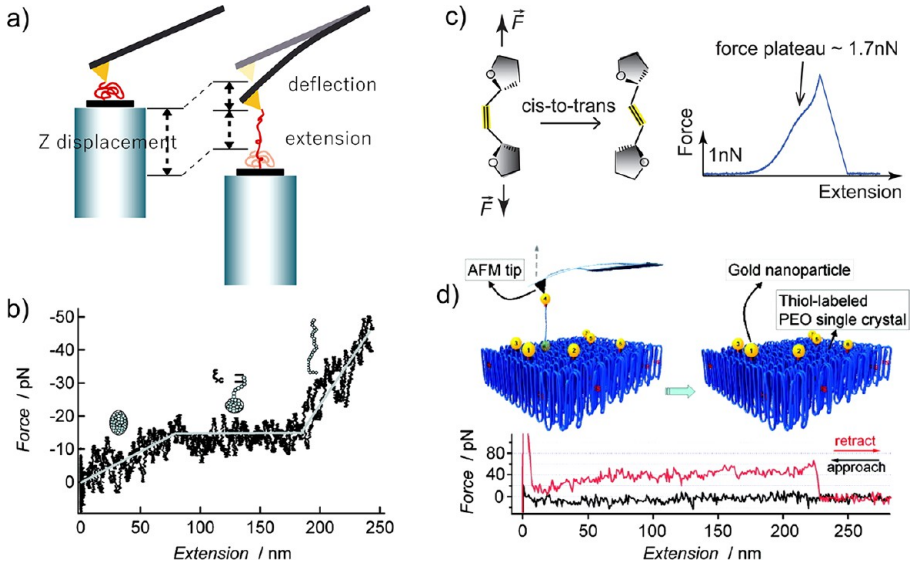

Figure 7. (a) Scheme of SMFS experiment. Reproduced with permission from ref 182. Copyright 2006 Elsevier. (b) A force plateau at ~13 pN is observed in the extension−retraction curve of an individual, collapsed PS chain in water. Black curve shows extension (pulling) of a single molecule and gray curve shows retraction (relaxation) process. Drawings along the curve illustrate the chain configurations of the extension of a single polymer chain in poor solvent. Reproduced with permission from ref 190. (c) Scheme of the force-induced rotation of carbon−carbon double bonds. Reproduced with permission from ref 200. (d) Scheme of extracting a single poly(ethylene oxide) chain from a single crystal by SMFS and corresponding force−extension curves. Reproduced with permission from ref 211.

casting that decreased to 5 nm after thermal annealing.[139] The presence of the amorphous surface layer has important consequences in the charge-transfer process. For polymer nanocomposites, related techniques were used to probe 50 nm gold particles buried in polymer matrix under ~1 μm.[142] The nondestructive subsurface imaging was also operated under an applied electric field, where the dispersion and orientation of CNTs in polymers were determined with nanometer-scale resolution.[143,144] These results provided in-depth morphological information and, hence, are expected to facilitate the analysis and preparation of polymer nanocomposites in the future.

Polymer Molecules Engineered Surface. AFM has played a key role in understanding surface modification by tethering various polymer molecules using grafting, self-assembly, or adsorption onto substrates.[145] The morphology of the engineered surfaces is critical in defining the properties. AFM topography imaging of such surface has quantified the morphologies and morphological transitions as functions of grafting density[146] and thickness of grafted layers.[147,148] The thickness of the engineered layers especially for polymer brush modified surface is often used to quantify structural changes as a function of solvents, pH, temperature, and ionic strength. AFM has subangstrom height resolution and, therefore, can measure the layer thickness fast and accurately by cross-section analysis of the polymer covered and uncovered regions.[149] Recently, AFM force−distance curve measurements were used to determine the layer thickness.[150−152] The applied loading force should must be considered when using AFM to measure the layer thickness, especially with compliant polymer layers, since the deformation of the polymers will cause errors in the measured height values.[153,154] For polymer brush modified surfaces, average molecular weights of the brush were determined by measuring the heights of the brushes in a good solvent in comparison to the known monomer length.[155]

Stimuli-Responsive Behavior. AFM can be used to monitor *in situ* the changes in properties (such as adhesion, wetting, mechanical performance, and friction) of stimuli-responsive polymers in response to external stimuli, such as pH,[156,157] temperature,[155,158] ionic strength,[159] light,[160] etc. Here, well-known responsive poly(*N*-isopropylacrylamide) (PNIPAM)-based polymers[161] show a reversible coil to globule transition at the so-called lower critical solution temperature (LCST). Above the LCST, in the collapsed state, hydrophobic polymeric aggregates are seen at the polymer surface, causing an abrupt change in the average film thickness and a dramatic increase in the roughness.[155] This transition was also observed for end-grafted polymer chains that had been grown from surface-immobilized monomers.[162] The transition dynamics under external stimuli can be easily measured by simply tracking the height change. High-resolution AFM measurements of a poly(methacrylic acid) brush in response to pH changes showed swelling and collapse transitions that occur on the subsecond time frame.[157] During the transition, molecular chains rearranged to another equilibrium structure in response to the external stimulus, and when compared to the measured mechanical properties, the structure−mechanical property relationship was directly determined.[163] Such information provided a better understanding of the structural complexity and responsive behavior of these advanced stimuli-responsive polymer materials under external stimuli.

Self-healing polymers represent one of the forefronts in materials chemistry and engineering.[164] AFM can be employed to image the healing process of this stimuli-responsive polymers. AFM imaging of the morphology changes as a function of temperature or time showed the healing process, uncovering the importance of polymer mobility in the healing. These *in situ* AFM observations provided fundamental insights into the healing of the domain morphology at the nanoscale.[165,166]

Polymer Chain Conformation. *In situ* visualization of single polymer chains and their motions have long been a challenge in polymer science.[167,168] Until recently, AFM imaging of a polystyrene-*b*-poly(methyl methacrylate) (PS-*b*-

DOI: 10.1021/acs.macromol.7b01459
Macromolecules 2018, 51, 3−24

PMMA) BCP LB film first visualized random coil conformations of a single synthetic polymer chain frozen on a substrate (Figure 6a).[169] Shortly thereafter, various structures such as polymer brushes,[170] dendron polymers,[171] polyelectrolytes,[172] and star polymers[173] were observed. In a case study, AFM molecular imaging of branching in linear acrylate-based macromolecules provided direct and quantitative information about branching topology including length and distribution of branches, not accessible by other methods (shown in Figure 6b).[174] This capability was also verified in a study of solvent-free, supersoft, and superelastic polymer melts and networks prepared from bottlebrush macromolecules, in which AFM molecular imaging qualitatively corroborated the increase in diameter and rigidity of bottlebrushes with increasing of the degree of polymerization of side chains (Figure 6c–f).[170] Not only the static structure but also the dynamic movements, i.e., the conformational rearrangements, of isolated chains in various environments were visualized.[172,173,175,176] Such molecular-level information, including static conformations and dynamics of conformational transitions, has greatly improved our understanding of the physical properties of polymers.

MECHANICAL PROPERTIES BY AFM: FROM MOLECULE SCALE TO MESOSCOPIC SCALE

Polymer materials often exhibit heterogeneities in material characteristics and chemical composition which, as we drive toward ever decreasing feature sizes or thicknesses, understanding the characteristic length scales and dynamics of these heterogeneities becomes increasingly important. AFM serves as a tool to provide such characterization of the surface. Here, we focus on recent progress made with the SMFS and AFM nanomechanical mapping—two typical force measurements and studies of synthetic polymers.

Single-Molecule Force Spectroscopy (SMFS). The principles and use of SMFS can be found elsewhere.[177−182] In a typical experiment, a functionalized AFM tip is brought into contact with the sample surface, where polymer chains have adsorbed. A single molecule can be bound to the tip and the substrate, by physical adsorption, ligand−receptor interaction, or covalent bonding. The force as a function of the distance that the cantilever has traveled vertically is measured as the molecule is stretched and eventually debonds or breaks, as shown in Figure 7a. The resultant force−distance curves provide not only the strength of the binding interaction but also insights into the elastic properties, conformational changes, and the unfolding of stretched polymer chains with piconewton sensitivity and subnanometer accuracy. Shortly after the development of SMFS in a polysaccharides study,[183] extensive works on inter/intramolecular forces of various polymer systems were investigated.

SMFS studies have shown that at low forces (<100 pN) the mechanical behavior of polymer chains is mainly affected by its entropic elasticity, while at high force region, larger than 300 pN, it is mainly affected by the enthalpic elasticity.[184] The side chain effects on the elasticity of polymer chains showed that for polymers with the same backbone the chains with larger side groups showed higher stiffness.[185,186] Recent SMFS measurements on polymers with side chains of different lengths and shapes revealed that only long and bulky side chains affected the enthalpic elasticity of the chain.[184] While such studies directly correlate the molecular structure of the polymers to the mechanical properties of a single chain, translating this, in general, to macroscopic properties is still a challenge, though some success was obtained with a biomimetic designed polymer.[187] Here, the complete, asymmetric potential energy profile of the rupture and refolding of each monomeric module showed a correlation with the bulk mechanical behavior by DMA measurements.

Interactions between the solvent and polymer chains are also critical, as the aggregation state of polymer chains also affects the mechanical behavior of the polymer.[186,188−192] The formation of hydrogen bonds, the solvent quality, and the size of the solvent molecules, i.e., the excluded volume, will influence the measured elasticity of the single chain.[188,189,192] By measuring the elasticity in different solvents, information about type and strength of interactions between the polymer and small molecules can be determined. As would be expected, with a polyelectrolyte, the charge density on the chain plays a critical role in its elasticity.[193] For PS chains, however, the elasticity constant was found to be the same for all different organic solvents investigated, but Kuhn length increased systematically with increasing solvent quality, reflecting the larger extent of swelling of the polymer in good solvents.[192]

Force-induced conformational transitions of single polymer chains can provide fundamental information about internal structure.[194,195] SMFS measurements of a PS chain in water, for example, showed three regions of the mechanical response corresponding to chain extension (retraction) and a force-induced globule−coil transition of polymer chains (Figure 7b), providing definitive proof of theoretical predictions.[196,197] Here, the hydrophobic PS chains collapsed in water due to nonfavorable interactions with water,[191] manifesting a classic collapse mechanism where the hydrophobic domain size dictated the structure and dynamics of water near polymers.[198] Force-induced isomerization of the *gem*-dibromocyclopropane (*g*DBC) into 2,3-dibromoalkenes was observed during the stretching of a *g*DBC-functionalized polybutadiene.[199] The structural rearrangement indicated the localized stress could be relaxed in polymers and polymer networks under load.[199] More recently, force-induced *cis*-to-*trans* isomerization of carbon−carbon double bonds has been observed in several polymer systems (Figure 7c).[200,201] These SMFS results indicate unique possibilities to develop advanced force-responsive materials. SMFS measurements on a more complex polymer system forced unfolding of single-chain polymer nanoparticles (SCNPs), provided insights into the interior structure of SCNPs, and by analysis of rupture events observed in the force profiles afforded insights into the assembly mechanism of the SCNPs.[202] Force-inducted structural transitions also provided important structural information on cross-linked polysaccharides[203] and disassembling block copolymer and micelles.[204,205]

SMFS can also provide quantitative information about intra/intermolecular interactions of polymer molecules[177,180,206,207] as well as desorption forces of polymer chains from the substrate surface.[193,208,209] Most SMFS studies on intermolecular interactions have focused on biological samples, since such interactions dictate the self-assembly process and direct the assembly of molecular building blocks into organized supramolecular structures, which is key for biological processes. Nonuniform force plateaus were observed when carboxymethycellulose (CMC) molecules were pulled out of a polymer film into a poor solvent and were described by a geometric model that involves the polymer−polymer and polymer−solvent interactions.[210] Recent SMFS studies on the pull-out of a single poly(ethylene oxide) (PEO) chain from a single crystal (shown in Figure 7d)[211] clearly demonstrated the adjacent re-

DOI: 10.1021/acs.macromol.7b01459
Macromolecules 2018, 51, 3−24

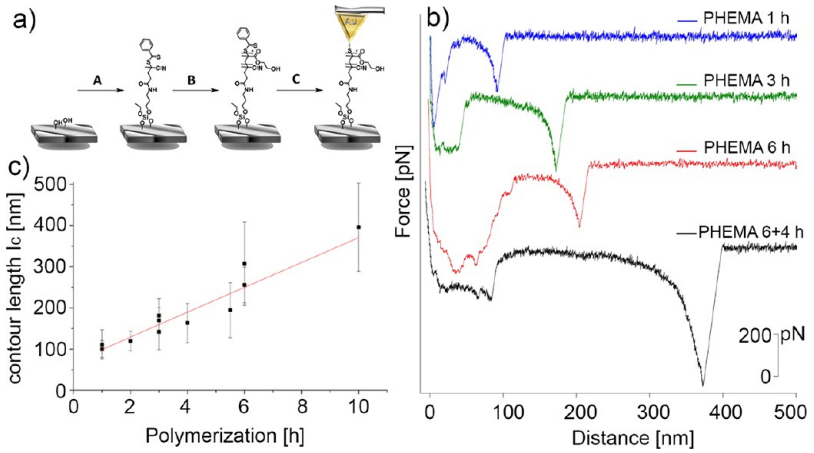

Figure 8. (a) Scheme of SMFS mapping of RAFT-controlled macromolecular growth. (b) Typical force−distance curves of poly(hydroxyethyl methacrylate) (PHEMA) strands that have different chain length. (c) Plot of contour length of the PHEMA chains versus polymerization time. Reproduced with permission from ref 215.

entry of the PEO chains in the single crystal prepared from dilute solution.[212]

SMFS has also been used to the determine molecular weight, molecular weight distribution, and grafting density[150,213] of surface-grafted polymers,[150,213−215] which has been a long-standing challenge.[145] SMFS results for a polycation, poly[2-(dimethylamino)ethyl methacrylate] (PDMAEMA), grafted from a poly(methyl methacrylate) (PMMA) backbone were shown to be consistent with results from gel permeation chromatography.[214] SMFS mapping on RAFT controlled macromolecular growth on glass surfaces showed the RAFT chain extension linearly with time up to high conversions (Figure 8), providing critical insight into macromolecular growth of the surface-initiated polymerization.[215]

AFM Nanomechanical Mapping (AFM-NMM). AFM-based NMM modes, such as force modulation,[216] force volume,[27,217] lateral force microscopy (also known as friction force microscopy),[218] contact resonance,[219] peak force tapping,[220,221] nanoindentation,[222,223] multifrequency force microscopy,[5] and also tapping mode phase imaging,[224] provide sample properties while simultaneously imaging the topography. A versatile and widely used approach among these is the force−distance (FD) curve-based imaging where an AFM tip scans over a specified area of the sample surface, and the corresponding applied force versus tip displacement is determined. Using appropriate contact mechanics models, such as the Hertz,[225] Johnson−Kendall−Roberts (JKR),[226] and Derjaguin−Muller−Toropov (DMT) models,[227] the 2D FD images can be translated into an areal mapping of the surface mechanical properties, including the elastic modulus, adhesion, dissipation, and stiffness. By simultaneously providing microstructure and mechanical properties with nanometer resolution and piconewton sensitivity, AFM-NMM has become a routine tool for probing polymer structure and determining local mechanical properties. Several pioneering studies using AFM-NMM on polymers have been published.[3,4,16,19,21,216]

The mechanical properties of thin and ultrathin polymer films are of critical importance for many applications, ranging from coatings to organic electronics. AFM-based nanoindentation measurements on thin polymer films supported on a noncompliant substrates showed that the effective out-of-plane modulus increases with decreasing film thickness when it is smaller than a threshold film thickness.[228−230] This enhancement of the elastic modulus can be explained by the propagation of the indentation-induced stress field and the interactions between the thin film and the underlying substrate.[230,231] The indentation-induced stress field propagation was found by measuring the elastic modulus of linear PS (LPS) and star-shaped PS (SPS). This was more evident for SPS than the LPS, indicating a more efficiently "packing" of the SPS, allowing a more efficient stress transfer.[231] Interactions between the thin film and the substrate were also found to affect the elastic modulus of the thin films. AFM nanoindentation simulations on the interfacial mechanical properties near attractive interfaces of supported PMMA thin films indicated that there was a gradient of local modulus with larger values near the substrate compared to the bulk, giving rise to interfacial confinement effects.[232] Force volume NMM measurements on rubbery poly(vinyl acetate) (PVAc) thin films further revealed the intermolecular interactions induced by nanoconfinement significantly affected the elastic and viscoelastic responses of polymers.[233] The above results provided important insights into the origin of the thickness-dependent mechanical properties of thin polymer films.

Characterization of the microstructure and mechanical properties at interfaces in polymer blends and composites has been a long-standing academic and technological challenge, since they dictate the ultimate properties. Studies on polystyrene/poly(*n*-butyl methacrylate) (PS/PnBMA) blends using AFM-NMM showed a gradual decrease in the Young's modulus from that of PS to that of PnBMA, clearly demarking the interfacial region.[234] AFM-NMM measurements of the reactive compatibilization of polyolefin elastomer (POE)/polyamide (PA6) blends demonstrated an interfacial reaction induced roughening and simultaneously afforded the strength and width of the interface.[235] The ability to map the spatial distribution of Young's modulus at an interface provides an alternate, efficient means of characterizing interfaces. This, of course, enables the investigation of polymer−polymer interdiffusion (shown in Figure 9);[221,236] polymer−fullerene nanoparticle interdiffusion;[237] compatibilized polymer blends where increased interfacial interactions of immiscible polymers mediated by an ionic liquid were revealed;[238] fiber reinforced polymer composites;[239] and carbon black reinforced rubber nanocomposites, where the thickness and elastic properties of the bound rubber phase were observed[240] and confirmed by

DOI: 10.1021/acs.macromol.7b01459
Macromolecules 2018, 51, 3−24

simulations.[241] Given the importance of the interface in defining properties of polymer blends and composites, AFM-NMM provides a unique view.

There has been much interest in the deformation mechanism of various polymers since the roles of molecular orientation and deformation-induced structural changes have been found to be of particular importance for the ultimate properties of a polymer. Although X-ray diffraction/scattering was widely used to probe the local molecular structure and structural dynamics of various polymers during deformation, they provide only structural information that is averaged over the area irradiated with the X-ray beam. With AFM real-space imaging, considerable information regarding polymer chain orientation, structural transition and dynamics, and fracture under deformation can be visualized. Such studies, using contact or tapping mode AFM, have been performed on semicrystalline polymers,[242−244] elastomeric polyolefins,[245,246] thermoplastic vulcanizates,[247] and stretchable electronic devices.[248] The real-space features of uniaxially stretched iPP sheets observed with frequency-modulation AFM were successfully compared with the X-ray scattering results obtained by synchrotron X-ray scattering.[249] Not only structural information but also the mechanical properties associated with structural developments under deformation are also of interest. Several recent studies using AFM-NMM have been performed on polymer hydrogels,[250] semicrystalline polymers,[251,252] and elastomers.[253,254] In a case study, AFM-NMM measurements on the structural evolution and mechanical properties of a deformed isoprene rubber (IR) clearly demonstrated a hierarchical nanofibrillar structure, ranging from several to a hundred nanometers in size, comprised of fibers oriented parallel to the stretching direction (Figure 10). The nanofibers, connected by oriented amorphous tie chains, form a network structure that was responsible for significantly enhanced stress, a key factor giving rise to the self-reinforcement of IR.[253]

Information about the viscoelastic properties at the nanoscale is another essential characteristics of polymeric materials and also an emerging area of AFM investigation. As discussed earlier, viscoelastic measurements using several AFM modes (e.g., force modulation, lateral force microscopy) have shown that there is a surface mobile layer with a reduced T_g in comparison to the bulk. With FD curve measurements, AFM-NMM, by analyzing changes in the pull-off forces in the vicinity of the glass transition, provided a means to determine the T_g of the topmost polymer layer.[55,255] Not only T_g, FD measurements on glass-to-rubber transition of amorphous polymers could be used to estimate the parameters of the Williams−Landel−Ferry equation and the Young's modulus and the yielding force of the polymer in a wide range of temperatures (70 K) and probe rates (6 decades), and the results are in very good agreement with measurements performed with customary techniques, such as broadband spectroscopy and dynamic mechanical analysis (DMA).[256] In more recent studies, viscoelastic properties can be mapped into a 2D image with nanometer spatial resolution.[257] As a case study, the viscoelastic properties including the storage modulus, loss modulus, and tan δ of styrene−butadiene rubber (SBR), IR, and a SBR/IR 7/3 blend were estimated and visualized from 1 Hz to 20 kHz using a recently developed nanorheology mapping technique.[258] These quantities obtained by AFM were in agreement with those measured using bulk DMA. Through this evaluation, nanorheology mapping has been shown to be a highly promising AFM mode for quantitative characterization of viscoelastic materials at the nanoscale, and its benefit to the research and development of small-scale compliant materials is expected to be substantial.

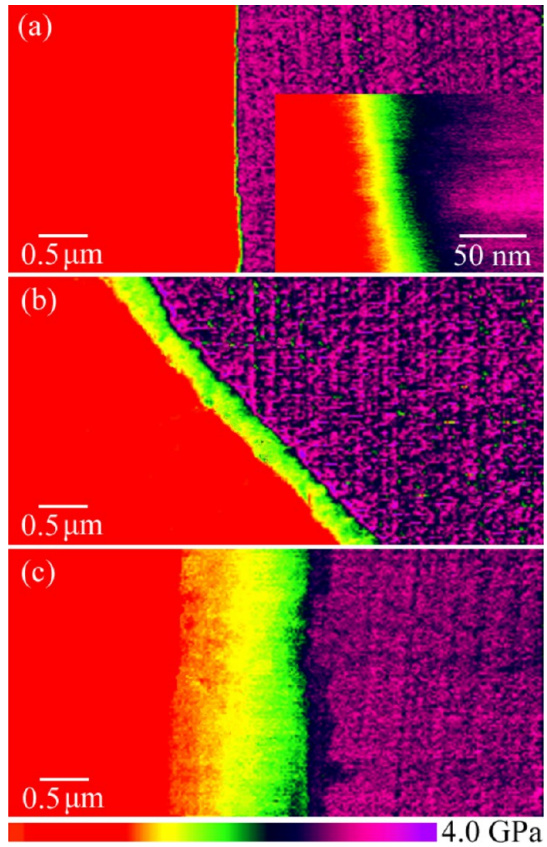

Figure 9. AFM-NMM Young's modulus maps of the miscible poly(vinyl chloride)/poly(caprolactone) sample annealed at 72 °C for (a) 5, (b) 20, and (c) 50 min. Reproduced with permission from ref 221.

In view of the increased importance of tribological properties (friction, lubrication, and wear) of the surfaces and interfaces of polymeric materials in lubrication, M/NEMS (micro/nano electromechanical devices), biomedical implants, and others, a molecular-level understanding of such tribology behavior is of special interest[259,260] and an increasingly active area of AFM-NMM investigation.[261−263] Early work on estimation of nanotribological properties by AFM-NMM has been shown for polymer blends,[264] thermoplastics,[265] and glassy polymers,[218] but most recent work has been focused on polymer brushes[266−269] because of their unique properties, such as reversible switching behavior, multivalent functionalization, tunable wettability, and lubrication. In most cases, several FD curve-based AFM-NMM techniques, such as lateral force and chemical force microscopies, are combined to estimate the tribological properties, for example, friction, adhesive, and elastic properties with nanometer resolution and under a wide variety of conditions. AFM-NMM measurements of the nanomechanical and nanotribological properties of polyelectrolyte brushes provided insights into how the Young's modulus and coefficient of friction can be tuned by varying the pH of the surroundings and the degree of physical or chemical cross-linking.[267] For polymer brush measurements, it is crucial to use colloidal probes because of their well-defined tip geometry and, therefore, can have a good match between the measured force−distance curves and theoretical models to

DOI: 10.1021/acs.macromol.7b01459
Macromolecules 2018, 51, 3−24

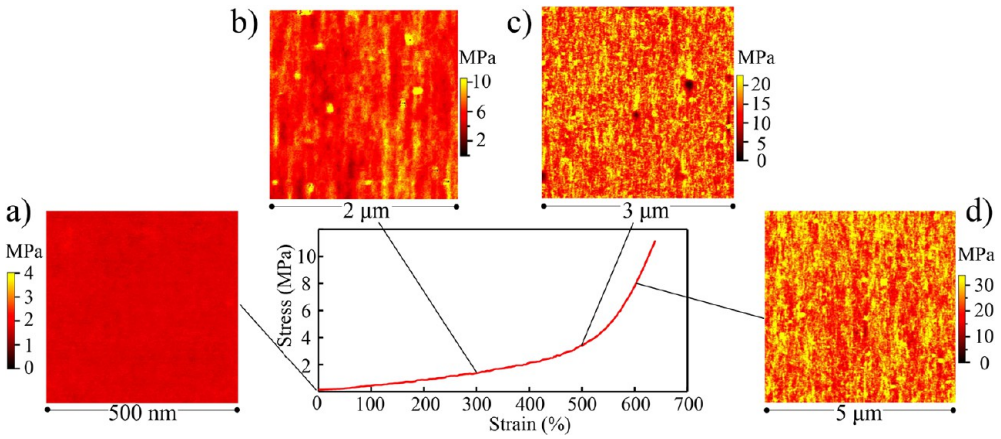

Figure 10. AFM-NMM images of stress distribution of isoprene rubber (IR) visualized structural evolution with strain 0% (a), 300% (b), 500% (c), and 600% (d). The strain is applied in the vertical direction of these images. Reproduced with permission from ref 253.

get mechanical properties accurately. This is also true for AFM measurements on mechanical properties of gels, which is increasingly important polymeric materials.

The importance of AFM-NMM was also demonstrated in other polymer systems, such as polymer nanofibers, where, by measuring the nanoscale mechanical properties of single fibers, the packing density and structural heterogeneity could be determined;[270−273] stimuli-responsive polymers such as PNIPAM that shows a well-known temperature-induced conformation transition at LCST, where the nanomechanical properties below and above the LCST, as well as on the dry state, were addressed;[274,275] semicrystalline polymers, in which the crystalline regions covered by a thin amorphous layer, were revealed;[276,277] and block copolymers, in which various local nanomechanical properties, not only Young's modulus but also adhesion and energy dissipation, were evaluated.[278−281]

NANOSCALE ELECTRICAL AND ELECTRONIC PROPERTIES BY AFM

Polymer-based solar cells (PSCs) have attracted significant attention from both academia and industry due to their semiconducting properties and potential for low-cost, flexible devices for alternative energy sources.[282−284] For PSC devices, donor/acceptor blends absorb photons to generate excitons, which then migrate to the donor/acceptor interfaces where they dissociate into free charge carriers. This process is dependent on nanoscopic details of the morphology, which is dependent on the chemical compositions and processing conditions.[285,286] Advanced AFM modes including conductive AFM (c-AFM), photoconductive AFM (pc-AFM), and scanning Kelvin probe force microscopy (KPFM) have been used to gain an understanding of the structure−performance relationship for the active layer of PSCs.[287−291] c-AFM, a derivative of AFM contact mode, characterizes the electrical characteristics with a typical spatial resolution of 10−20 nm. In this mode, a dc bias is applied between the conductive tip and sample while the tip scans over the sample surface, and information about the nanoscale topography and current distribution (conductivity) is recorded simultaneously. Studies using c-AFM clearly visualized, as evidenced by current distribution map, the phase-separated donor and acceptor regions and the electron- and hole-transport networks.[292−296] Heterogeneous conductive regions smaller than 20 nm were detected.[297] The thermal annealing induced heterogeneous conductivity in poly(3-hexylthiophene) (P3HT) thin films[297,298] increased hole and electron mobilities in P3HT/[6,6]-phenyl C61-butyric acid methyl ester (PCBM) blends[292] and decreased the width of the interface between the donor and acceptor regions.[296] The use of solvent additives resulted in a finely phase-separated morphology[295] as evidenced by c-AFM. Consequently, the processing conditions that determine the morphology of the active layer could be directly correlated with the PSC performance.

Similar to the force−distance curves, current−voltage ($I-V$) curves can also be extracted from c-AFM and provide some underlying information on electron conductivity and mobility of the nanostructures, such as the hole mobilities of P3HT in neat P3HT films,[294,299] in poly(3-alkylthiophene) (P3AT) nanofibers,[300] or in P3HT:PCBM blends,[292] which could never be determined by macroscopic $J-V$ measurements. It should be noted that there may be a large discrepancy between the charge carrier mobility measured with c-AFM and that measured by a macroscopic planar device[299,301] due to the geometric differences between the two experiments and the areas over which the different methods average.[299] Using a semiempirical equation proposed by Reid et al.,[299] however, reliable mobilities can be extracted, allowing the measurement of local mobilities with nanoscale resolution in the heterogeneous films used in light-emitting diodes, transistors, and solar cells.

It is more interesting, however, to obtain information on the photocurrent generation at the nanoscale that can be used to correlate with charge generation, transport, and collection that dominate bulk device performance. pc-AFM, a derivative of c-AFM but with the addition of a diffraction-limited laser source to illuminate the device (Figure 11a), has been used to resolve the complex optoelectronic and morphological phenomena of PSCs with a typical resolution of 10−20 nm.[302−309] Photocurrent mapping of a poly[2-methoxy-5-(3′,7′-dimethyloctyloxy)-1,4-phenylenevinylene] (MDMO-PPV)/PCBM film gave evidence for two length scales of heterogeneities arising from the solvent casting conditions (shown in Figure 11).[302] In P3HT:PCBM films, pc-AFM data showed significant inhomogeneities on the length scale of 100−500 nm, arising from local variations at the surface, not reflecting the bulk organization.[304] In a high-performance PTB7:PCBM blend, pc-AFM revealed a bulk heterojunction (BHJ) structure consisting of elongated PCBM-rich and PTB7-rich fiber-like domains, 10−50 nm wide and 200−400 nm long, indicating that the formation of narrow

DOI: 10.1021/acs.macromol.7b01459
Macromolecules 2018, 51, 3−24

and elongated domains is desirable for efficient BHJ solar cells.[309] Moreover, not only the surface but also the subsurface morphology can be revealed by pc-AFM, with an estimated depth resolution of ~20 nm within the P3HT:PCBM film.[307]

KPFM, a noncontact variant of AFM, can be used to probe local surface potentials (work function) to local morphologies with a resolution better than 10 nm.[310,311] KPFM is contactless, which is an important when dealing with soft organic thin films. Early studies of MDMO–PPV/PCBM blends using KPFM identified a barrier for electron transmission from the electron-rich PCBM nanoclusters toward the extracting cathode.[312] In polyfluorene-based photodiodes, KPFM revealed the presence of a capping layer that reduces the efficiency of the photovoltaic device by blocking the transport of photogenerated electrons to the surface.[313] With improved resolution down to sub-10 nm, surface morphologies of the interpenetrated networks of P3HT:PCBM blends are clearly evident, and the carrier generation at the donor–acceptor interfaces and their transport through the percolation pathways in the nanometer range have been directly visualized.[310] KPFM studies on P3HT-*b*-P3MT and P3HT nanofibers showed that the surface potential, related to the work function of the sample, is very sensitive to the nanostructure morphology resulting from a combined effect of chain-packing disorder, molecular weight, and local environment.[314,315] The decay of the surface potential into the film was determined on the ~millisecond scale, which suggested an intensity-dependent recombination kinetics that is in quantitative agreement with the carrier recombination kinetics measured in bulk devices.[316]

The combination of AFM-based techniques, such as c-AFM, pc-AFM, and KPFM, provides comprehensive characteristics of the local morphology and the electrical and optoelectronic properties of PSCs, thereby establishing a direct correlation of local heterogeneities within the nanostructure and photocurrent generation in the bulk device.[287−291] Studies in P3HT/PCBM blend devices showed that the thermal annealing-induced morphological heterogeneities, as seen in the distribution maps of local current (by c-AFM) and short-circuit photocurrent (by pc-AFM), may lead to the imperfect internal quantum efficiency of some blends.[303] In a poly(3-butylthiophene) (P3BT):PCBM blend device, the direct connections between local nanostructure and overall device performance, as shown in the local current and photocurrent maps, showed that the nanostructure, controlled by using a combination of thermal and solvent annealing, is the single most important variable determining the device performance,[305] while in a P3HT nanowire:PCBM blend devices, the results demonstrated the importance of vertical morphology within the active layer on the device performance.[306] Copolymer-based devices, in contrast to the physically mixed polymer:fullerene blends, are inherently microphased separated on the tens of nanometers level, underscoring the importance of molecular design and morphological control that determine the nature of the self-assembled nanostructures for developing highly efficient polymer:fullerene PSCs.[308] Since c-AFM and pc-AFM are operated in contact mode, c-AFM and pc-AFM still face challenges including scan-induced damage,[306] injection/extraction barriers due to the work function of the tip,[317] and difficulty in making quantitative comparisons with the external quantum efficiency (EQE) of the macroscopic diode.

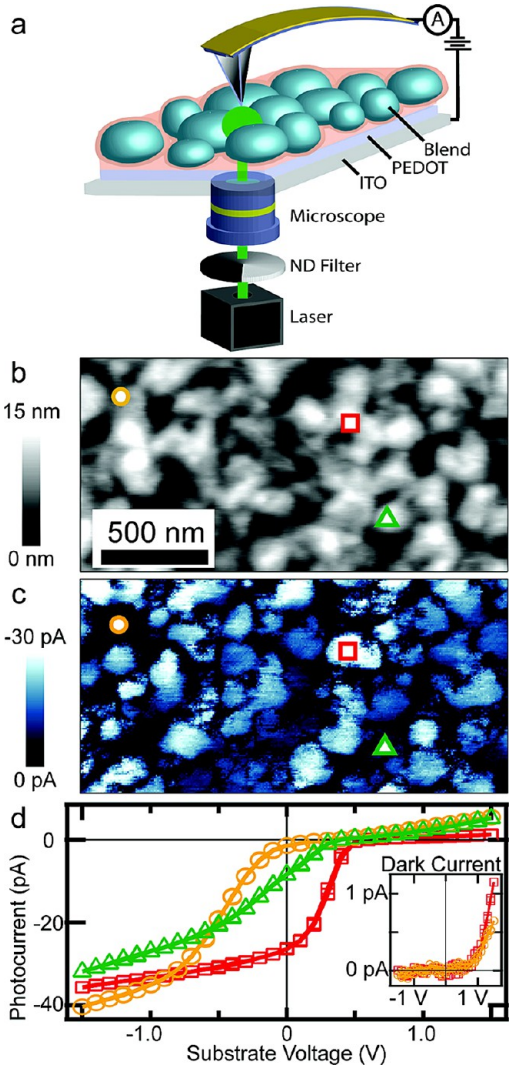

Figure 11. (a) Schematic of the pc-AFM setup. pc-AFM height image (b) and photocurrent map (c) of a MDMO-PPV:PCBM 20:80 thin film. (d) Local current–applied voltage curves acquired at three locations shown in (b) and (c). Inset: local current–voltage curves without illumination showing much smaller dark currents. Reproduced with permission from ref 302.

■ PROSPECTS

The past 30 years have seen considerable impact of AFM on our understanding of polymers. With the advances of multiparametric and multifunctional characterization with high resolution and the capacity to operate under various media, AFM is well positioned to tackle the challenges of understanding the structure and properties of increasingly more complex polymers and their composites. In measurement developments, for example, multifrequency AFM is emerging and provides a promising framework to improve compositional sensitivity and spatial and time resolution of materials in their native environment.[318] In a case study, bimodal AFM (one kind of multifrequency AFM) imaging of metallopolymer-grafted diblock copolymers clearly revealed a lamellar morphology featuring a spherical substructure for the polyvinylferrocene (PVFc) segments inside the polyisoprene lamellae.[319] The morphological structure of the grafted diblock copolymer measured by bimodal AFM is in excellent agreement with the TEM and SAXS,[319] indicating the high sensitivity for

DOI: 10.1021/acs.macromol.7b01459
Macromolecules 2018, 51, 3−24

compositional heterogeneities well suited for the high-resolution imaging of polymers. Combining AFM with existing techniques, in particular chemistry related characterizing methods, put AFM at an even more advanced level. AFM-IR, combining AFM and infrared spectroscopy, opens a door to nanoscale chemical characterization, where the spatial variation in infrared absorption and reflection with up to a 15 nm resolution is possible.[14,320,321] This advance paves the way for new insights into the underlying structure beyond phenomenological physical responses (e.g., dissipation and mechanical properties), of a wide range of polymer materials, such as polymer blends, composites, fibers, and thin films for active devices, such as organic photovoltaics. Several recent studies using AFM-IR have shed some light on the structures and compositions with micro- and nanoscale feature sizes,[322−324] which were not been possible by either conventional IR or AFM. The capabilities of AFM-IR, with the addition of some other accessories, such as a polarization control, can be further extended to probe the orientation in anisotropic supramolecular assemblies.[325] The combination of AFM with mass spectrometry (MS) for topographical and chemical imaging of polymer systems has also emerged very recently.[326,327] Moreover, the combination of two or more AFM-based modes to characterize multiple aspects of polymers is another promising way to characterize polymers with exceptional spatial resolution. Such a combination, for example, AFM and scanning electrochemical microscopy (AFM-SCEM), provided spatially correlated electrochemical and nanomechanical information paired with high-resolution topographical data of soft electronic devices.[328] It is evident that such combinations will allow AFM methods to meet the challenges posed by increasing complexity in structure and function of polymer materials.

Despite the wealth of information AFM provides, an important limitation is the relatively slow data acquisition times that lead to difficulty in following many dynamic processes and structural transitions of polymers occurring on the nano- to microseconds time scale. Although recently commercialized high-speed AFM (HS-AFM), which allows images to be collected at video rates, has provided new insights into the nanostructural dynamics and dynamic processes of biological samples,[15,329] its application to polymeric systems has been limited, since it requires relatively large tip−sample forces to keep constant tip−sample contact. With improved force and drift control systems, HS-AFM would make a considerable impact on our understanding of structural dynamics of polymers, such as polymer crystal growth and BCP assembly. Another unresolved, also the most important, issue for high-precision AFM images and absolute property measurements is developing an understanding of tip−sample interactions and modeling (e.g., contact mechanics modeling, tip shape modeling, etc.). For example, AFM-NMM, by applying some contact mechanics models such as JKR or DMT, etc., has been widely used to quantitatively measure the nanoscale mechanical properties of polymer materials. However, these continuum contact models have many assumptions.[28] Depending on the tip shape, contact radius, strength of tip−sample adhesion, and softness of sample, the assumptions of these models are essential to understand to interpret the force−distance curves accurately.[31,32,330] Recent work has shown that blunt tips must be used to get valid absolute values of mechanical properties.[30,331] With the continuous development in understandings of the tip−sample interaction and modeling, improvements in spatial and temporal resolution, multiparametric and multifunctional characterization, advances in AFM should lead to a more comprehensive understanding of the dynamic, structural, mechanical, chemical, and functional heterogeneity of complex polymer systems and allow one to address outstanding questions in polymers in the coming decades.

AUTHOR INFORMATION

Corresponding Author

*E-mail: dwang@mail.buct.edu.cn (D.W.).

ORCID

Dong Wang: 0000-0003-2326-0852

Thomas P. Russell: 0000-0001-6384-5826

Notes

The authors declare no competing financial interest.

Biographies

Dong Wang received his Ph.D. in Materials Science and Engineering in 2008 from Tsinghua University. He was a Research Associate at the Tohoku University (2008−2011), an Assistant Professor (2011−2015) at the same institution, working with Professor Toshio Nishi (now in the Tokyo Institute of Technology (TIT)) and Professor Ken Nakajima (now also in the TIT), and a Visiting Scholar at the University of Massachusetts Amherst (2012−2013), working with Professor Thomas P. Russell. Since 2015, he has been a full professor in the College of Material Sciences and Engineering at the Beijing University of Chemical Technology (BUCT). His current research focuses on polymer surface and interface characterization using AFM-based techniques.

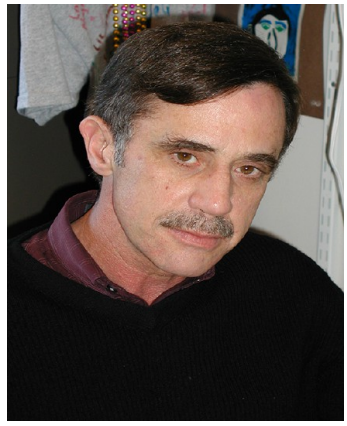

Thomas P. Russell, the Silvio O. Conte Distinguished Professor of Polymer Science and Engineering at the University of Massachusetts in Amherst, received his PhD in 1979 from the same institution. He was a Research Associate at the University of Mainz (1979−1981) and a

DOI: 10.1021/acs.macromol.7b01459
Macromolecules 2018, 51, 3−24

Research Staff Member at the IBM Almaden Research Center in San Jose, CA (1981−1996), and became a Professor of Polymer Science and Engineering at the University of Massachusetts Amherst (1997). He is also a Visiting Faculty at the Materials Sciences Division in the Lawrence Berkeley National Laboratory, an Adjunct Professor at the Beijing University of Chemical Technology, and a lead PI at the Advanced Institute of Materials Research at Tohoku University. He was the Director of the Materials Research Science and Engineering Center from 1996−2009 and the Director of the Energy Frontier Research Center on Polymer-Based Materials for Harvesting Solar Energy (2009−2014) and is a lead PI in the WPI-Advanced Institute of Materials Research at Tohoku University (2006−present), the Global Research Laboratory at Seoul National University (2005−2015), and the Beijing Advanced Innovation Center on Soft Matter (2016−present). He is a Fellow of the American Physical Society, Materials Research Society, Neutron Scattering Society of America, American Association for the Advancement of Science, and the American Chemical Society, Polymer Materials Science and Engineering Division. He has received the Polymer Physic Prize of the APS, the Cooperative Research Award of the ACS, the Dutch Polymer Award, the ACS Award in Applied Polymer Science, and the Society of Polymer Science Japan International Award and is an elected member of the National Academy of Engineering. He is also an Associate Editor of *Macromolecules*.

REFERENCES

(1) Binnig, G.; Quate, C. F.; Gerber, C. Atomic Force Microscope. *Phys. Rev. Lett.* **1986**, *56*, 930−933.

(2) Magonov, S. N.; Whangbo, M. H. *Surface Analysis with STM and AFM: Experimental and Theoretical Aspects of Image Analysis*, 1st ed.; Wiley-VCH: New York, 1996.

(3) Vancso, G. J.; Schönherr, H. *Scanning Force Microscopy of Polymers*; Springer: Berlin, 2010.

(4) Tsukruk, V. V.; Singamaneni, S. *Scanning Probe Microscopyof Soft Matter: Fundamentals and Practices*; Wiley-VCH Verlag GmbH & Co. KGaA: 2011.

(5) Garcia, R.; Herruzo, E. T. The Emergence of Multifrequency Force Microscopy. *Nat. Nanotechnol.* **2012**, *7*, 217−226.

(6) Garcia, R.; Knoll, A. W.; Riedo, E. Advanced Scanning Probe Lithography. *Nat. Nanotechnol.* **2014**, *9*, 577−587.

(7) Gerber, C.; Lang, H. P. How the Doors to the Nanoworld Were Opened. *Nat. Nanotechnol.* **2006**, *1*, 3−5.

(8) Dufrene, Y. F.; Ando, T.; Garcia, R.; Alsteens, D.; Martinez-Martin, D.; Engel, A.; Gerber, C.; Muller, D. J. Imaging Modes of Atomic Force Microscopy for Application in Molecular and Cell Biology. *Nat. Nanotechnol.* **2017**, *12*, 295−307.

(9) Chiefari, J.; Chong, Y. K.; Ercole, F.; Krstina, J.; Jeffery, J.; Le, T. P. T.; Mayadunne, R. T. A.; Meijs, G. F.; Rizzardo, E.; Thang, S. H. Living Free-Radical Polymerization by Reversible Addition-Fragmentation Chain Transfer: The RAFT Process. *Macromolecules* **1998**, *31*, 5559−5562.

(10) Arriola, D. J.; Carnahan, E. M.; Hustad, P. D.; Kuhlman, R. L.; Wenzel, T. T. Catalytic Production of Olefin Block Copolymers Via Chain Shuttling Polymerization. *Science* **2006**, *312*, 714−719.

(11) Matyjaszewski, K. Atom Transfer Radical Polymerization (ATRP): Current Status and Future Perspectives. *Macromolecules* **2012**, *45*, 4015−4039.

(12) Ando, T. High-Speed Atomic Force Microscopy Coming of Age. *Nanotechnology* **2012**, *23*, 062001.

(13) Hammiche, A.; Pollock, H. M.; Reading, M.; Claybourn, M.; Turner, P. H.; Jewkes, K. Photothermal FT-IR Spectroscopy: A Step Towards FT-IR Microscopy at a Resolution Better Than the Diffraction Limit. *Appl. Spectrosc.* **1999**, *53*, 810−815.

(14) Dazzi, A.; Prater, C. B. AFM-IR: Technology and Applications in Nanoscale Infrared Spectroscopy and Chemical Imaging. *Chem. Rev.* **2017**, *117*, 5146−5173.

(15) Uchihashi, T.; Iino, R.; Ando, T.; Noji, H. High-Speed Atomic Force Microscopy Reveals Rotary Catalysis of Rotorless F_1-ATPase. *Science* **2011**, *333*, 755−758.

(16) Cappella, B.; Dietler, G. Force-Distance Curves by Atomic Force Microscopy. *Surf. Sci. Rep.* **1999**, *34*, 1−104.

(17) García, R.; Pérez, R. Dynamic Atomic Force Microscopy Methods. *Surf. Sci. Rep.* **2002**, *47*, 197−301.

(18) Giessibl, F. J. Advances in Atomic Force Microscopy. *Rev. Mod. Phys.* **2003**, *75*, 949−983.

(19) Butt, H. J.; Cappella, B.; Kappl, M. Force Measurements with the Atomic Force Microscope: Technique, Interpretation and Applications. *Surf. Sci. Rep.* **2005**, *59*, 1−152.

(20) Garcia, R. *Amplitude Modulation Atomic Force Microscopy*; Wiley-VCH Verlag GmbH & Co. KGaA: Weinheim, Germany, 2010.

(21) McConney, M. E.; Singamaneni, S.; Tsukruk, V. V. Probing Soft Matter with the Atomic Force Microscopies: Imaging and Force Spectroscopy. *Polym. Rev.* **2010**, *50*, 235−286.

(22) Radmacher, M.; Tillamnn, R. W.; Fritz, M.; Gaub, H. E. From Molecules to Cells: Imaging Soft Samples with the Atomic Force Microscope. *Science* **1992**, *257*, 1900−1905.

(23) Zhang, S.; Aslan, H.; Besenbacher, F.; Dong, M. Quantitative Biomolecular Imaging by Dynamic Nanomechanical Mapping. *Chem. Soc. Rev.* **2014**, *43*, 7412−7429.

(24) García, R.; San Paulo, A. Attractive and Repulsive Tip-Sample Interaction Regimes in Tapping-Mode Atomic Force Microscopy. *Phys. Rev. B: Condens. Matter Mater. Phys.* **1999**, *60*, 4961−4967.

(25) García, R.; San Paulo, A. Amplitude Curves and Operating Regimes in Dynamic Atomic Force Microscopy. *Ultramicroscopy* **2000**, *82*, 79−83.

(26) Knoll, A.; Magerle, R.; Krausch, G. Tapping Mode Atomic Force Microscopy on Polymers: Where Is the True Sample Surface? *Macromolecules* **2001**, *34*, 4159−4165.

(27) Wang, D.; Fujinami, S.; Nakajima, K.; Nishi, T. True Surface Topography and Nanomechanical Mapping Measurements on Block Copolymers with Atomic Force Microscopy. *Macromolecules* **2010**, *43*, 3169−3172.

(28) Johnson, K. L.; Greenwood, J. A. An Adhesion Map for the Contact of Elastic Spheres. *J. Colloid Interface Sci.* **1997**, *192*, 326−333.

(29) Kopycinska-Muller, M.; Geiss, R. H.; Hurley, D. C. Contact Mechanics and Tip Shape in AFM-Based Nanomechanical Measurements. *Ultramicroscopy* **2006**, *106*, 466−474.

(30) Dokukin, M. E.; Sokolov, I. On the Measurements of Rigidity Modulus of Soft Materials in Nanoindentation Experiments at Small Depth. *Macromolecules* **2012**, *45*, 4277−4288.

(31) Dokukin, M. E.; Sokolov, I. Quantitative Mapping of the Elastic Modulus of Soft Materials with Harmonix and Peakforce QNM AFM Modes. *Langmuir* **2012**, *28*, 16060−16071.

(32) Chyasnavichyus, M.; Young, S. L.; Tsukruk, V. V. Probing of Polymer Surfaces in the Viscoelastic Regime. *Langmuir* **2014**, *30*, 10566−10582.

(33) Magonov, S. N.; Elings, V.; Whangbo, M. H. Phase Imaging and Stiffness in Tapping-Mode Atomic Force Microscopy. *Surf. Sci.* **1997**, *375*, L385−L391.

(34) Cleveland, J. P.; Anczykowski, B.; Schmid, A. E.; Elings, V. B. Energy Dissipation in Tapping-Mode Atomic Force Microscopy. *Appl. Phys. Lett.* **1998**, *72*, 2613−2615.

(35) Paulo, Á. S.; García, R. Tip-Surface Forces, Amplitude, and Energy Dissipation in Amplitude-Modulation (Tapping Mode) Force Microscopy. *Phys. Rev. B: Condens. Matter Mater. Phys.* **2001**, *64*, 193411.

(36) Gómez, C. J.; Garcia, R. Determination and Simulation of Nanoscale Energy Dissipation Processes in Amplitude Modulation AFM. *Ultramicroscopy* **2010**, *110*, 626−633.

(37) Magonov, S. N.; Reneker, D. H. Characterization of Polymer Surfaces with Atomic Force Microscopy. *Annu. Rev. Mater. Sci.* **1997**, *27*, 175−222.

(38) Ediger, M. D.; Forrest, J. A. Dynamics near Free Surfaces and the Glass Transition in Thin Polymer Films: A View to the Future. *Macromolecules* **2014**, *47*, 471−478.

DOI: 10.1021/acs.macromol.7b01459
Macromolecules 2018, 51, 3−24

(39) Keddie, J. L.; Jones, R. A. L.; Cory, R. A. Size-Dependent Depression of the Glass Transition Temperature in Polymer Films. *Europhys. Lett.* **1994**, *27*, 59−64.
(40) Serghei, A.; Huth, H.; Schick, C.; Kremer, F. Glassy Dynamics in Thin Polymer Layers Having a Free Upper Interface. *Macromolecules* **2008**, *41*, 3636−3639.
(41) Kim, H.; Rühm, A.; Lurio, L. B.; Basu, J. K.; Lal, J.; Lumma, D.; Mochrie, S. G. J.; Sinha, S. K. Surface Dynamics of Polymer Films. *Phys. Rev. Lett.* **2003**, *90*, 068302.
(42) Tanaka, K.; Taura, A.; Ge, S. R.; Takahara, A.; Kajiyama, T. Molecular Weight Dependence of Surface Dynamic Viscoelastic Properties for the Monodisperse Polystyrene Film. *Macromolecules* **1996**, *29*, 3040−3042.
(43) Kerle, T.; Lin, Z.; Kim, H. C.; Russell, T. P. Mobility of Polymers at the Air/Polymer Interface. *Macromolecules* **2001**, *34*, 3484−3492.
(44) Fakhraai, Z.; Forrest, J. A. Measuring the Surface Dynamics of Glassy Polymers. *Science* **2008**, *319*, 600−604.
(45) Ilton, M.; Qi, D.; Forrest, J. A. Using Nanoparticle Embedding to Probe Surface Rheology and the Length Scale of Surface Mobility in Glassy Polymers. *Macromolecules* **2009**, *42*, 6851−6854.
(46) Yang, Z.; Fujii, Y.; Lee, F. K.; Lam, C. H.; Tsui, O. K. Glass Transition Dynamics and Surface Layer Mobility in Unentangled Polystyrene Films. *Science* **2010**, *328*, 1676−1679.
(47) Wang, D.; Liu, Y.; Nishi, T.; Nakajima, K. Length Scale of Mechanical Heterogeneity in a Glassy Polymer Determined by Atomic Force Microscopy. *Appl. Phys. Lett.* **2012**, *100*, 251905.
(48) Chai, Y.; Salez, T.; McGraw, J. D.; Benzaquen, M.; Dalnoki-Veress, K.; Raphaël, E.; Forrest, J. A. A Direct Quantitative Measure of Surface Mobility in a Glassy Polymer. *Science* **2014**, *343*, 994−999.
(49) Zhang, W.; Yu, L. Surface Diffusion of Polymer Glasses. *Macromolecules* **2016**, *49*, 731−735.
(50) Kajiyama, T.; Tanaka, K.; Takahara, A. Surface Molecular Motion of the Monodisperse Polystyrene Films. *Macromolecules* **1997**, *30*, 280−285.
(51) Tanaka, K.; Takahara, A.; Kajiyama, T. Rheological Analysis of Surface Relaxation Process of Monodisperse Polystyrene Films. *Macromolecules* **2000**, *33*, 7588−7593.
(52) Mayes, A. M. Glass Transition of Amorphous Polymer Surfaces. *Macromolecules* **1994**, *27*, 3114−3115.
(53) Ngai, K. L.; Rizos, A. K.; Plazek, D. J. Reduction of the Glass Temperature of Thin Freely Standing Polymer Films Caused by the Decrease of the Coupling Parameterin the Coupling Model. *J. Non-Cryst. Solids* **1998**, *235-237*, 435−443.
(54) Brown, H.; Russell, T. P. Entanglements at Polymer Surfaces and Interfaces. *Macromolecules* **1996**, *29*, 798−800.
(55) Bliznyuk, V. N.; Assender, H. E.; Briggs, G. A. D. Surface Glass Transition Temperature of Amorphous Polymers. A New Insight with SFM. *Macromolecules* **2002**, *35*, 6613−6622.
(56) Yang, Z.; Clough, A.; Lam, C. H.; Tsui, O. K. C. Glass Transition Dynamics and Surface Mobility of Entangled Polystyrene Films at Equilibrium. *Macromolecules* **2011**, *44*, 8294−8300.
(57) Qi, D.; Ilton, M.; Forrest, J. A. Measuring Surface and Bulk Relaxation in Glassy Polymers. *Eur. Phys. J. E: Soft Matter Biol. Phys.* **2011**, *34*, 56.
(58) Yoon, H.; McKenna, G. B. Substrate Effects on Glass Transition and Free Surface Viscoelasticity of Ultrathin Polystyrene Films. *Macromolecules* **2014**, *47*, 8808−8818.
(59) Qi, D.; Fakhraai, Z.; Forrest, J. A. Substrate and Chain Size Dependence of near Surface Dynamics of Glassy Polymers. *Phys. Rev. Lett.* **2008**, *101*, 096101.
(60) Ge, S.; Pu, Y.; Zhang, W.; Rafailovich, M.; Sokolov, J.; Buenviaje, C.; Buckmaster, R.; Overney, R. M. Shear Modulation Force Microscopy Study of near Surface Glass Transition Temperatures. *Phys. Rev. Lett.* **2000**, *85*, 2340−2343.
(61) Ediger, M. D.; Angell, C. A.; Nagel, S. R. Supercooled Liquids and Glasses. *J. Phys. Chem.* **1996**, *100*, 13200−13212.
(62) Debenedetti, P. G.; Stillinger, F. H. Supercooled Liquids and the Glass Transition. *Nature* **2001**, *410*, 259−267.
(63) Chandler, D. Liquids: Condensed, Disordered, and Sometimes Complex. *Proc. Natl. Acad. Sci. U. S. A.* **2009**, *106*, 15111−15112.
(64) Garrahan, J. P. Dynamic Heterogeneity Comes to Life. *Proc. Natl. Acad. Sci. U. S. A.* **2011**, *108*, 4701−4702.
(65) Liu, A. J.; Nagel, S. R. The Jamming Transition and the Marginally Jammed Solid. *Annu. Rev. Condens. Matter Phys.* **2010**, *1*, 347−369.
(66) Berthier, L.; Biroli, G.; Bouchaud, J. P.; Cipelletti, L.; Saarloos, W. V. *Dynamical Heterogeneities in Glasses, Colloids, and Granular Media*; Oxford University Press: Oxford, 2011.
(67) Russell, E. V.; Israeloff, N. E. Direct Observation of Molecular Cooperativity near the Glass Transition. *Nature* **2000**, *408*, 695−698.
(68) Siretanu, I.; Saadaoui, H.; Chapel, J.-P.; Drummond, C. Spatial Heterogeneity of Glassy Polymer Films. *Macromolecules* **2015**, *48*, 2787−2792.
(69) Adam, G.; Gibbs, J. H. On the Temperature Dependence of Cooperative Relaxation Properties in Glass-Forming Liquids. *J. Chem. Phys.* **1965**, *43*, 139−146.
(70) Hempel, E.; Hempel, G.; Hensel, A.; Schick, C.; Donth, E. Characteristic Length of Dynamic Glass Transition near T_g for a Wide Assortment of Glass-Forming Substances. *J. Phys. Chem. B* **2000**, *104*, 2460−2466.
(71) Nguyen, H. K.; Wang, D.; Russell, T. P.; Nakajima, K. Observation of Dynamical Heterogeneities and Their Time Evolution on the Surface of an Amorphous Polymer. *Soft Matter* **2015**, *11*, 1425−1433.
(72) Hobbs, J. K.; Farrance, O. E.; Kailas, L. How Atomic Force Microscopy Has Contributed to Our Understanding of Polymer Crystallization. *Polymer* **2009**, *50*, 4281−4292.
(73) Pearce, R.; Vancso, G. J. Imaging of Melting and Crystallization of Poly(Ethylene Oxide) in Real-Time by Hot-Stage Atomic Force Microscopy. *Macromolecules* **1997**, *30*, 5843−5848.
(74) Pearce, R.; Vancso, G. J. Real-Time Imaging of Melting and Crystallization in Poly(Ethylene Oxide) by Atomic Force Microscopy. *Polymer* **1998**, *39*, 1237−1242.
(75) Hobbs, J. K.; McMaster, T. J.; Miles, M. J.; Barham, P. J. Direct Observations of the Growth of Spherulites of Poly(Hydroxybutyrate-co-Valerate) Using Atomic Force Microscopy. *Polymer* **1998**, *39*, 2437−2446.
(76) Schultz, J. M.; Miles, M. J. AFM Study of Morphological Development During the Melt-Crystallization of Poly(Ethylene Oxide). *J. Polym. Sci., Part B: Polym. Phys.* **1998**, *36*, 2311−2325.
(77) Liu, Y. X.; Chen, E. Q. Polymer Crystallization of Ultrathin Films on Solid Substrates. *Coord. Chem. Rev.* **2010**, *254*, 1011−1037.
(78) Reiter, G.; Strobl, G. R. *Progress in Understanding of Polymer Crystallization*; Springer: Berlin, 2007.
(79) Beekmans, L. G. M.; Vancso, G. J. Real-Time Crystallization Study of Poly(ε-Caprolactone) by Hot-Stage Atomic Force Microscopy. *Polymer* **2000**, *41*, 8975−8981.
(80) Zhou, J. J.; Liu, J. G.; Yan, S. K.; Dong, J. Y.; Li, L.; Chan, C. M.; Schultz, J. M. Atomic Force Microscopy Study of the Lamellar Growth of Isotactic Polypropylene. *Polymer* **2005**, *46*, 4077−4087.
(81) Lei, Y. G.; Chan, C. M.; Li, J. X.; Ng, K. M.; Wang, Y.; Jiang, Y.; Li, L. The Birth of an Embryo and Development of the Founding Lamella of Spherulites as Observed by Atomic Force Microscopy. *Macromolecules* **2002**, *35*, 6751−6753.
(82) Li, L.; Chan, C. M.; Yeung, K. L.; Li, J. X.; Ng, K. M.; Lei, Y. Direct Observation of Growth of Lamellae and Spherulites of a Semicrystalline Polymer by AFM. *Macromolecules* **2001**, *34*, 316−325.
(83) Hugel, T.; Strobl, G.; Thomann, R. Building Lamellae from Blocks: The Pathway Followed in the Formation of Crystallites of Syndiotactic Polypropylene. *Acta Polym.* **1999**, *50*, 214−217.
(84) Magonov, S.; Godovsky, Y. Atomic Force Microscopy-Part 8: Visualization of Granular Nanostructure in Crystalline Polymers. *Am. Lab.* **1999**, *31*, 52−58.
(85) Strobl, G. From the Melt Via Mesomorphic and Granular Crystalline Layers to Lamellar Crystallites: A Major Route Followed in Polymer Crystallization? *Eur. Phys. J. E: Soft Matter Biol. Phys.* **2000**, *3*, 165−183.

DOI: 10.1021/acs.macromol.7b01459
Macromolecules 2018, 51, 3−24

(86) Strobl, G. A Thermodynamic Multiphase Scheme Treating Polymer Crystallization and Melting. *Eur. Phys. J. E: Soft Matter Biol. Phys.* **2005**, *18*, 295−309.
(87) Strobl, G. Crystallization and Melting of Bulk Polymers: New Observations, Conclusions and a Thermodynamic Scheme. *Prog. Polym. Sci.* **2006**, *31*, 398−442.
(88) Xu, J.; Guo, B. H.; Zhang, Z. M.; Zhou, J. J.; Jiang, Y.; Yan, S.; Li, L.; Wu, Q.; Chen, G. Q.; Schultz, J. M. Direct AFM Observation of Crystal Twisting and Organization in Banded Spherulites of Chiral Poly(3-Hydroxybutyrate-co-3-Hydroxyhexanoate). *Macromolecules* **2004**, *37*, 4118−4123.
(89) Gazzano, M.; Focarete, M. L.; Riekel, C.; Scandola, M. Bacterial Poly(3-Hydroxybutyrate): An Optical Microscopy and Microfocus X-Ray Diffraction Study. *Biomacromolecules* **2000**, *1*, 604−608.
(90) Keith, H. D.; Padden, J. F. J. Twisting Orientation and the Role of Transient States in Polymer Crystallization. *Polymer* **1984**, *25*, 28−42.
(91) Lotz, B.; Cheng, S. Z. D. A Critical Assessment of Unbalanced Surface Stresses as the Mechanical Origin of Twisting and Scrolling of Polymer Crystals. *Polymer* **2005**, *46*, 577−610.
(92) Toda, A.; Okamura, M.; Taguchi, K.; Hikosaka, M.; Kajioka, H. Branching and Higher Order Structure in Banded Polyethylene Spherulites. *Macromolecules* **2008**, *41*, 2484−2493.
(93) Toda, A.; Taguchi, K.; Kajioka, H. Instability-Driven Branching of Lamellar Crystals in Polyethylene Spherulites. *Macromolecules* **2008**, *41*, 7505−7512.
(94) Kumaki, J.; Kawauchi, T.; Yashima, E. Two-Dimensional Folded Chain Crystals of a Synthetic Polymer in a Langmuir-Blodgett Film. *J. Am. Chem. Soc.* **2005**, *127*, 5788−5789.
(95) Anzai, T.; Kawauchi, M.; Kawauchi, T.; Kumaki, J. Crystallization Behavior of Single Isotactic Poly(Methyl Methacrylate) Chains Visualized by Atomic Force Microscopy. *J. Phys. Chem. B* **2015**, *119*, 338−347.
(96) Takanashi, Y.; Kumaki, J. Significant Melting Point Depression of Two-Dimensional Folded-Chain Crystals of Isotactic Poly(Methyl Methacrylate)s Observed by High-Resolution in Situ Atomic Force Microscopy. *J. Phys. Chem. B* **2013**, *117*, 5594−5605.
(97) Mullin, N.; Hobbs, J. K. Direct Imaging of Polyethylene Films at Single-Chain Resolution with Torsional Tapping Atomic Force Microscopy. *Phys. Rev. Lett.* **2011**, *107*, 197801.
(98) Savage, R. C.; Mullin, N.; Hobbs, J. K. Molecular Conformation at the Crystal−Amorphous Interface in Polyethylene. *Macromolecules* **2015**, *48*, 6160−6165.
(99) Frank, F. C. General Introduction. *Faraday Discuss. Chem. Soc.* **1979**, *68*, 7−13.
(100) Yoon, D. Y.; Flory, P. J. Small-Angle Neutron Scattering by Semicrystalline Polyethylene. *Polymer* **1977**, *18*, 509−513.
(101) Wang, D.; Liu, F.; Yagihashi, N.; Nakaya, M.; Ferdous, S.; Liang, X.; Muramatsu, A.; Nakajima, K.; Russell, T. P. New Insights into Morphology of High Performance BHJ Photovoltaics Revealed by High Resolution AFM. *Nano Lett.* **2014**, *14*, 5727−5732.
(102) Kozub, D. R.; Vakhshouri, K.; Orme, L. M.; Wang, C.; Hexemer, A.; Gomez, E. D. Polymer Crystallization of Partially Miscible Polythiophene/Fullerene Mixtures Controls Morphology. *Macromolecules* **2011**, *44*, 5722−5726.
(103) Collin, B.; Chatenay, D.; Coulon, G.; Ausserre, D.; Gallot, Y. Ordering of Copolymer Thin Films as Revealed by Atomic Force Microscopy. *Macromolecules* **1992**, *25*, 1621−1622.
(104) McLean, R. S.; Sauer, B. B. Tapping-Mode AFM Studies Using Phase Detection for Resolution of Nanophases in Segmented Polyurethanes and Other Block Copolymers. *Macromolecules* **1997**, *30*, 8314−8317.
(105) Knoll, A.; Horvat, A.; Lyakhova, K. S.; Krausch, G.; Sevink, G. J.; Zvelindovsky, A. V.; Magerle, R. Phase Behavior in Thin Films of Cylinder-Forming Block Copolymers. *Phys. Rev. Lett.* **2002**, *89*, 035501.
(106) Park, C.; Yoon, J.; Thomas, E. L. Enabling Nanotechnology with Self Assembled Block Copolymer Patterns. *Polymer* **2003**, *44*, 6725−6760.
(107) Darling, S. B. Directing the Self-Assembly of Block Copolymers. *Prog. Polym. Sci.* **2007**, *32*, 1152−1204.
(108) Meuler, A. J.; Hillmyer, M. A.; Bates, F. S. Ordered Network Mesostructures in Block Polymer Materials. *Macromolecules* **2009**, *42*, 7221−7250.
(109) Li, W.; Müller, M. Directed Self-Assembly of Block Copolymers by Chemical or Topographical Guiding Patterns: Optimizing Molecular Architecture, Thin-Film Properties, and Kinetics. *Prog. Polym. Sci.* **2016**, *54*−*55*, 47−75.
(110) Yufa, N. A.; Li, J.; Sibener, S. J. In-Situ High-Temperature Studies of Diblock Copolymer Structural Evolution. *Macromolecules* **2009**, *42*, 2667−2671.
(111) Tsarkova, L.; Horvat, A.; Krausch, G.; Zvelindovsky, A. V.; Sevink, G. J. A.; Magerle, R. Defect Evolution in Block Copolymer Thin Films Via Temporal Phase Transitions. *Langmuir* **2006**, *22*, 8089−8095.
(112) Hahm, J.; Lopes, W. A.; Jaeger, H. M.; Sibener, S. J. Defect Evolution in Ultrathin Films of Polystyrene-block-Polymethylmethacrylate Diblock Copolymers Observed by Atomic Force Microscopy. *J. Chem. Phys.* **1998**, *109*, 10111.
(113) Hammond, M. R.; Cochran, E.; Fredrickson, G. H.; Kramer, E. J. Temperature Dependence of Order, Disorder, and Defects in Laterally Confined Diblock Copolymer Cylinder Monolayers. *Macromolecules* **2005**, *38*, 6575−6585.
(114) Horvat, A.; Sevink, G. J. A.; Zvelindovsky, A. V.; Krekhov, A.; Tsarkova, L. Specific Features of Defect Structure and Dynamics in the Cylinder Phase of Block Copolymers. *ACS Nano* **2008**, *2*, 1143−1152.
(115) Harrison, C.; Adamson, D. H.; Cheng, Z.; Sebastian, J. M.; Sethuraman, S.; Huse, D. A.; Register, R. A.; Chaikin, P. M. Mechanisms of Ordering in Striped Patterns. *Science* **2000**, *290*, 1558−1560.
(116) Mishra, V.; Fredrickson, G. H.; Kramer, E. J. Effect of Film Thickness and Domain Spacing on Defect Densities Indirected Self-Assembly of Cylindrical Morphology Block Copolymers. *ACS Nano* **2012**, *6*, 2629−2641.
(117) Olszowka, V.; Hund, M.; Kuntermann, V.; Scherdel, S.; Tsarkova, L.; Böker, A. Electric Field Alignment of a Block Copolymer Nanopattern: Direct Observation of the Microscopic Mechanism. *ACS Nano* **2009**, *3*, 1091−1096.
(118) Knoll, A.; Lyakhova, K. S.; Horvat, A.; Krausch, G.; Sevink, G. J.; Zvelindovsky, A. V.; Magerle, R. Direct Imaging and Mesoscale Modelling of Phase Transitions in a Nanostructured Fluid. *Nat. Mater.* **2004**, *3*, 886−891.
(119) Horvat, A.; Knoll, A.; Krausch, G.; Tsarkova, L.; Lyakhova, K. S.; Sevink, G. J. A.; Zvelindovsky, A. V.; Magerle, R. Time Evolution of Surface Relief Structures in Thin Block Copolymer Films. *Macromolecules* **2007**, *40*, 6930−6939.
(120) Tsarkova, L.; Knoll, A.; Magerle, R. Rapid Transitions between Defect Configurations in a Block Copolymer Melt. *Nano Lett.* **2006**, *6*, 1574−1577.
(121) Tong, Q.; Sibener, S. J. Visualization of Individual Defect Mobility and Annihilation within Cylinder-Forming Diblock Copolymer Thin Films on Nanopatterned Substrates. *Macromolecules* **2013**, *46*, 8538−8544.
(122) Kataoka, K.; Harada, A.; Nagasaki, Y. Block Copolymer Micelles for Drug Delivery: Design, Characterization and Biological Significance. *Adv. Drug Delivery Rev.* **2001**, *47*, 113−131.
(123) Discher, D. E.; Eisenberg, A. Polymer Vesicles. *Science* **2002**, *297*, 967−973.
(124) Van Zanten, J. H.; Monbouquette, H. G. Characterization of Vesicles by Classical Light Scattering. *J. Colloid Interface Sci.* **1991**, *146*, 330−336.
(125) Šlouf, M.; Lapčíková, M.; Štěpánek, M. Imaging of Block Copolymer Vesicles in Solvated State by Wet Scanning Transmission Electron Microscopy. *Eur. Polym. J.* **2011**, *47*, 1273−1278.
(126) Regenbrecht, M.; Akari, S.; Förster, S.; Möhwald, H. Shape Investigations of Charged Block Copolymer Micelles on Chemically Different Surfaces by Atomic Force Microscopy. *J. Phys. Chem. B* **1999**, *103*, 6669−6675.

DOI: 10.1021/acs.macromol.7b01459
Macromolecules 2018, 51, 3−24

(127) Webber, G. B.; Wanless, E. J.; Armes, S. P.; Baines, F. L.; Biggs, S. Adsorption of Amphiphilic Diblock Copolymer Micelles at the Mica/Solution Interface. *Langmuir* **2001**, *17*, 5551−5561.
(128) Hamley, I. W.; Connell, S. D.; Collins, S. In Situ Atomic Force Microscopy Imaging of Adsorbed Block Copolymer Micelles. *Macromolecules* **2004**, *37*, 5337−5351.
(129) Alekseev, A.; Efimov, A.; Loos, J.; Matsko, N.; Syurik, J. Three-Dimensional Imaging of Polymer Materials by Scanning Probe Tomography. *Eur. Polym. J.* **2014**, *52*, 154−165.
(130) Jinnai, H.; Spontak, R. J.; Nishi, T. Transmission Electron Microtomography and Polymer Nanostructures. *Macromolecules* **2010**, *43*, 1675−1688.
(131) Zhong, Y.; Trinh, M. T.; Chen, R.; Purdum, G. E.; Khlyabich, P. P.; Sezen, M.; Oh, S.; Zhu, H.; Fowler, B.; Zhang, B.; Wang, W.; Nam, C. Y.; Sfeir, M. Y.; Black, C. T.; Steigerwald, M. L.; Loo, Y. L.; Ng, F.; Zhu, X. Y.; Nuckolls, C. Molecular Helices as Electron Acceptors in High-Performance Bulk Heterojunction Solar Cells. *Nat. Commun.* **2015**, *6*, 8242.
(132) Magerle, R. Nanotomography. *Phys. Rev. Lett.* **2000**, *85*, 2749−2752.
(133) Franke, M.; Rehse, N. Three-Dimensional Structure Formation of Polypropylene Revealed by in Situ Scanning Force Microscopy and Nanotomography. *Macromolecules* **2008**, *41*, 163−166.
(134) Dietz, C.; Zerson, M.; Riesch, C.; Gigler, A. M.; Stark, R. W.; Rehse, N.; Magerle, R. Nanotomography with Enhanced Resolution Using Bimodal Atomic Force Microscopy. *Appl. Phys. Lett.* **2008**, *92*, 143107.
(135) Alekseev, A.; Efimov, A.; Lu, K.; Loos, J. Three-Dimensional Electrical Property Mapping with Nanometer Resolution. *Adv. Mater.* **2009**, *21*, 4915−4919.
(136) Efimov, A. E.; Gnaegi, H.; Schaller, R.; Grogger, W.; Hofer, F.; Matsko, N. B. Analysis of Native Structures of Soft Materials by Cryo Scanning Probe Tomography. *Soft Matter* **2012**, *8*, 9756−9760.
(137) Liedel, C.; Hund, M.; Olszowka, V.; Böker, A. On the Alignment of a Cylindrical Block Copolymer: A Time-Resolved and 3-Dimensional SFM Study. *Soft Matter* **2012**, *8*, 995−1002.
(138) Tetard, L.; Passian, A.; Venmar, K. T.; Lynch, R. M.; Voy, B. H.; Shekhawat, G.; Dravid, V. P.; Thundat, T. Imaging Nanoparticles in Cells by Nanomechanical Holography. *Nat. Nanotechnol.* **2008**, *3*, 501−505.
(139) Zerson, M.; Spitzner, E. C.; Riesch, C.; Lohwasser, R.; Thelakkat, M.; Magerle, R. Subsurface Mapping of Amorphous Surface Layers on Poly(3-Hexylthiophene). *Macromolecules* **2011**, *44*, 5874−5877.
(140) Spitzner, E.-C.; Riesch, C.; Szilluweit, R.; Tian, L.; Frauenrath, H.; Magerle, R. Multi-Set Point Intermittent Contact (MUSIC) Mode Atomic Force Microscopy of Oligothiophene Fibrils. *ACS Macro Lett.* **2012**, *1*, 380−383.
(141) Ebeling, D.; Eslami, B.; Solares, S. D. J. Visualizing the Subsurface of Soft Matter: Simultaneous Topographical Imaging, Depth Modulation, and Compositional Mapping with Triple Frequency Atomic Force Microscopy. *ACS Nano* **2013**, *7*, 10387−10396.
(142) Kimura, K.; Kobayashi, K.; Matsushige, K.; Yamada, H. Imaging of Au Nanoparticles Deeply Buried in Polymer Matrix by Various Atomic Force Microscopy Techniques. *Ultramicroscopy* **2013**, *133*, 41−49.
(143) Phang, I. Y.; Liu, T.; Zhang, W. D.; Schönherr, H.; Vancso, G. J. Probing Buried Carbon Nanotubes within Polymer−Nanotube Composite Matrices by Atomic Force Microscopy. *Eur. Polym. J.* **2007**, *43*, 4136−4142.
(144) Thompson, H. T.; Barroso-Bujans, F.; Herrero, J. G.; Reifenberger, R.; Raman, A. Subsurface Imaging of Carbon Nanotube Networks in Polymers with DC-Biased Multifrequency Dynamic Atomic Force Microscopy. *Nanotechnology* **2013**, *24*, 135701.
(145) Sui, X.; Zapotoczny, S.; Benetti, E. M.; Schön, P.; Vancso, G. J. Characterization and Molecular Engineering of Surface-Grafted Polymer Brushes across the Length Scales by Atomic Force Microscopy. *J. Mater. Chem.* **2010**, *20*, 4981−4993.
(146) Wang, H.; Brown, H. R. Atomic Force Microscopy Study of the Photografting of Glycidyl Methacrylate onto HDPE and the Microstructure of the Grafted Chains. *Polymer* **2007**, *48*, 477−487.
(147) Luzinov, I.; Julthongpiput, D.; Tsukruk, V. V. Thermoplastic Elastomer Monolayers Grafted to a Functionalized Silicon Surface. *Macromolecules* **2000**, *33*, 7629−7638.
(148) Lim, E.; Tu, G.; Schwartz, E.; Cornelissen, J. J. L. M.; Rowan, A. E.; Nolte, R. J. M.; Huck, W. T. S. Synthesis and Characterization of Surface-Initiated Helical Polyisocyanopeptide Brushes. *Macromolecules* **2008**, *41*, 1945−1951.
(149) Shah, R. R.; Merreceyes, D.; Husemann, M.; Rees, I.; Abbott, N. L.; Hawker, C. J.; Hedrick, J. L. Using Atom Transfer Radical Polymerization to Amplify Aonolayers of Initiators Patterned by Microcontact Printing into Polymer Brushes for Pattern Transfer. *Macromolecules* **2000**, *33*, 597−605.
(150) Cuenot, S.; Gabriel, S.; Jérôme, R.; Jérôme, C.; Fustin, C. A.; Jonas, A. M.; Duwez, A.-S. First Insights into Electrografted Polymers by AFM-Based Force Spectroscopy. *Macromolecules* **2006**, *39*, 8428−8433.
(151) Cuellar, J. L.; Llarena, I.; Iturri, J. J.; Donath, E.; Moya, S. E. A Novel Approach for Measuring the Intrinsic Nanoscale Thickness of Polymer Brushes by Means of Atomic Force Microscopy: Application of a Compressible Fluid Model. *Nanoscale* **2013**, *5*, 11679−11685.
(152) Dokukin, M. E.; Kuroki, H.; Minko, S.; Sokolov, I. AFM Study of Polymer Brush Grafted to Deformable Surfaces: Quantitative Properties of the Brush and Substrate Mechanics. *Macromolecules* **2017**, *50*, 275−282.
(153) Lego, B.; Francois, M.; Skene, W. G.; Giasson, S. Polymer Brush Covalently Attached to OH-Functionalized Mica Surface Via Surface-Initiated ATRP: Control of Grafting Density and Polymer Chain Length. *Langmuir* **2009**, *25*, 5313−5321.
(154) Halperin, A.; Zhulina, E. B. Atomic Force Microscopy of Polymer Brushes: Colloidal Versus Sharp Tips. *Langmuir* **2010**, *26*, 8933−8940.
(155) Benetti, E. M.; Zapotoczny, S.; Vancso, G. J. Tunable Thermoresponsive Polymeric Platforms on Gold by "Photoiniferter"-Based Surface Grafting. *Adv. Mater.* **2007**, *19*, 268−271.
(156) Orlov, M.; Tokarev, I.; Scholl, A.; Doran, A.; Minko, S. pH-Responsive Thin Film Membranes from Poly(2-Vinylpyridine)-Water Vapor-Induced Formation of a Microporous Structure. *Macromolecules* **2007**, *40*, 2086−2091.
(157) Parnell, A. J.; Martin, S. J.; Jones, R. A. L.; Vasilev, C.; Crook, C. J.; Ryan, A. J. Direct Visualization of the Real Time Swelling and Collapse of a Poly(Methacrylic Acid) Brush Using Atomic Force Microscopy. *Soft Matter* **2009**, *5*, 296−299.
(158) Henn, D. M.; Fu, W.; Mei, S.; Li, C. Y.; Zhao, B. Temperature-Induced Shape Changing of Thermosensitive Binary Heterografted Linear Molecular Brushes between Extended Wormlike and Stable Globular Conformations. *Macromolecules* **2017**, *50*, 1645−1656.
(159) Murdoch, T. J.; Humphreys, B. A.; Willott, J. D.; Gregory, K. P.; Prescott, S. W.; Nelson, A.; Wanless, E. J.; Webber, G. B. Specific Anion Effects on the Internal Structure of a Poly(N-Isopropylacrylamide) Brush. *Macromolecules* **2016**, *49*, 6050−6060.
(160) Kopyshev, A.; Galvin, C. J.; Patil, R. R.; Genzer, J.; Lomadze, N.; Feldmann, D.; Zakrevski, J.; Santer, S. Light-Induced Reversible Change of Roughness and Thickness of Photosensitive Polymer Brushes. *ACS Appl. Mater. Interfaces* **2016**, *8*, 19175−19184.
(161) Schild, H. G. Poly(N-Isopropylacrylamide): Expriment, Theroy and Application. *Prog. Polym. Sci.* **1992**, *17*, 163−249.
(162) Ishida, N.; Biggs, S. Direct Observation of the Phase Transition for a Poly(N-Isopropylacryamide) Layer Grafted onto a Solid Surface by AFM and QCM-D. *Langmuir* **2007**, *23*, 11083−11088.
(163) Nalam, P. C.; Lee, H. S.; Bhatt, N.; Carpick, R. W.; Eckmann, D. M.; Composto, R. J. Nanomechanics of pH-Responsive, Drug-Loaded, Bilayered Polymer Grafts. *ACS Appl. Mater. Interfaces* **2017**, *9*, 12936−12948.
(164) Yang, Y.; Urban, M. W. Self-Healing Polymeric Materials. *Chem. Soc. Rev.* **2013**, *42*, 7446−7467.

DOI: 10.1021/acs.macromol.7b01459
Macromolecules 2018, 51, 3−24

(165) Yufa, N. A.; Li, J.; Sibener, S. J. Diblock Copolymer Healing. *Polymer* **2009**, *50*, 2630−2634.
(166) Yoon, J. A.; Kamada, J.; Koynov, K.; Mohin, J.; Nicolaÿ, R.; Zhang, Y.; Balazs, A. C.; Kowalewski, T.; Matyjaszewski, K. Self-Healing Polymer Films Based on Thiol−Disulfide Exchange Reactions and Self-Healing Kinetics Measured Using Atomic Force Microscopy. *Macromolecules* **2012**, *45*, 142−149.
(167) Sheiko, S. S.; Möller, M. Visualization of Macromolecules-a First Step to Manipulation and Controlled Response. *Chem. Rev.* **2001**, *101*, 4099−4123.
(168) Gallyamov, M. O. Scanning Force Microscopy as Applied to Conformational Studies in Macromolecular Research. *Macromol. Rapid Commun.* **2011**, *32*, 1210−1246.
(169) Kumaki, J.; Nishikawa, Y.; Hashimoto, T. Visualization of Single-Chain Conformations of a Synthetic Polymer with Atomic Force Microscopy. *J. Am. Chem. Soc.* **1996**, *118*, 3321−3322.
(170) Daniel, W. F. M.; Burdynska, J.; Vatankhah-Varnoosfaderani, M.; Matyjaszewski, K.; Paturej, J.; Rubinstein, M.; Dobrynin, A. V.; Sheiko, S. S. Solvent-Free, Supersoft and Superelastic Bottlebrush Melts and Networks. *Nat. Mater.* **2015**, *15*, 183−189.
(171) Percec, V.; Ahn, C. H.; Ungar, G.; Yeardley, D. J. P.; Möller, M.; Sheiko, S. S. Controlling Polymer Shape through the Self-Assembly of Dendritic Side-Groups. *Nature* **1998**, *391*, 161−164.
(172) Minko, S.; Kiriy, A.; Gorodyska, G.; Stamm, M. Single Flexible Hydrophobic Polyelectrolyte Molecules Adsorbed on Solid Substrate-Transition between a Stretched Chain, Necklace-Like Conformation and a Globule. *J. Am. Chem. Soc.* **2002**, *124*, 3218−3219.
(173) Kiriy, A.; Gorodyska, G.; Minko, S.; Stamm, M.; Tsitsilianis, C. Single Molecules and Associates of Heteroarm Star Copolymer Visualized by Atomic Force Microscopy. *Macromolecules* **2003**, *36*, 8704−8711.
(174) Yu-Su, S. Y.; Sun, F. C.; Sheiko, S. S.; Konkolewicz, D.; Lee, H.; Matyjaszewski, K. Molecular Imaging and Analysis of Branching Topology in Polyacrylates by Atomic Force Microscopy. *Macromolecules* **2011**, *44*, 5928−5936.
(175) Xu, H.; Shirvanyants, D.; Beers, K.; Matyjaszewski, K.; Rubinstein, M.; Sheiko, S. S. Molecular Motion in a Spreading Precursor Film. *Phys. Rev. Lett.* **2004**, *93*, 206103.
(176) Kumaki, J.; Kawauchi, T.; Yashima, E. Reptational Movements of Single Synthetic Polymer Chains on Substrate Observed by in-Situ Atomic Force Microscopy. *Macromolecules* **2006**, *39*, 1209−1215.
(177) Hugel, T.; Seitz, M. The Study of Molecular Interactions by AFM Force Spectroscopy. *Macromol. Rapid Commun.* **2001**, *22*, 989−1016.
(178) Zhang, W.; Zhang, X. Single Molecule Mechanochemistry of Macromolecules. *Prog. Polym. Sci.* **2003**, *28*, 1271−1295.
(179) Vancso, G. J. Feeling the Force of Supramolecular Bonds in Polymers. *Angew. Chem., Int. Ed.* **2007**, *46*, 3794−3796.
(180) Zhang, X.; Liu, C.; Wang, Z. Force Spectroscopy of Polymers: Studying on Intramolecular and Intermolecular Interactions in Single Molecular Level. *Polymer* **2008**, *49*, 3353−3361.
(181) Grebikova, L.; Radiom, M.; Maroni, P.; Schlüter, A. D.; Borkovec, M. Recording Stretching Response of Single Polymer Chains Adsorbed on Solid Substrates. *Polymer* **2016**, *102*, 350−362.
(182) Nakajima, K.; Watabe, H.; Nishi, T. Single Polymer Chain Rubber Elasticity Investigated by Atomic Force Microscopy. *Polymer* **2006**, *47*, 2505−2510.
(183) Rief, M.; Oesterhelt, F.; Heymann, B.; Gaub, H. E. Single Molecule Force Spectroscopy on Polysaccharides by Atomic Force Microscopy. *Science* **1997**, *275*, 1295−1297.
(184) Luo, Z.; Zhang, A.; Chen, Y.; Shen, Z.; Cui, S. How Big Is Big Enough? Effect of Length and Shape of Side Chains on the Single-Chain Enthalpic Elasticity of a Macromolecule. *Macromolecules* **2016**, *49*, 3559−3565.
(185) Zhang, W.; Zou, S.; Wang, C.; Zhang, X. Single Polymer Chain Elongation of Poly(N-Isopropylacrylamide) and Poly(Acrylamide) by Atomic Force Microscopy. *J. Phys. Chem. B* **2000**, *104*, 10258−10264.
(186) Wang, C.; Shi, W.; Zhang, W.; Zhang, X.; Katsumoto, Y.; Ozaki, Y. Force Spectroscopy Study on Poly(Acrylamide) Derivatives: Effects of Substitutes and Buffers on Single-Chain Elasticity. *Nano Lett.* **2002**, *2*, 1169−1172.
(187) Chung, J.; Kushner, A. M.; Weisman, A. C.; Guan, Z. Direct Correlation of Single-Molecule Properties with Bulk Mechanical Performance for the Biomimetic Design of Polymers. *Nat. Mater.* **2014**, *13*, 1055−1062.
(188) Zhang, Q.; Marszalek, P. E. Solvent Effects on the Elasticity of Polysaccharide Molecules in Disordered and Ordered States by Single-Molecule Force Spectroscopy. *Polymer* **2006**, *47*, 2526−2532.
(189) Luo, Z.; Zhang, B.; Qian, H. J.; Lu, Z. Y.; Cui, S. Effect of the Size of Solvent Molecules on the Single-Chain Mechanics of Poly(Ethylene Glycol): Implications on a Novel Design of a Molecular Motor. *Nanoscale* **2016**, *8*, 17820−17827.
(190) Gunari, N.; Balazs, A. C.; Walker, G. C. Force-Induced Globule-Coil Transition in Single Polystyrene Chains in Water. *J. Am. Chem. Soc.* **2007**, *129*, 10046−10047.
(191) Li, I. T. S.; Walker, G. C. Interfacial Free Energy Governs Single Polystyrene Chain Collapse in Water and Aqueous Solutions. *J. Am. Chem. Soc.* **2010**, *132*, 6530−6540.
(192) Radiom, M.; Maroni, P.; Borkovec, M. Influence of Solvent Quality on the Force Response of Individual Poly(Styrene) Polymer Chains. *ACS Macro Lett.* **2017**, 1052−1055.
(193) Hugel, T.; Grosholz, M.; Clausen-Schaumann, H.; Pfau, A.; Gaub, H.; Seitz, M. Elasticity of Single Polyelectrolyte Chains and Their Desorption from Solid Supports Studied by AFM Based Single Molecule Force Spectroscopy. *Macromolecules* **2001**, *34*, 1039−1047.
(194) Marszalek, P. E.; Oberhauser, A. F.; Pang, Y. P.; Fernandez, J. M. Polysaccharide Elasticity Governed by Chair-Boat Transitions of the Glucopyranose Ring. *Nature* **1998**, *396*, 661−664.
(195) Liu, C.; Wang, Z.; Zhang, X. Force Spectroscopy of Single-Chain Polysaccharides: Force-Induced Conformational Transition of Amylose Disappears under Environment of Micelle Solution. *Macromolecules* **2006**, *39*, 3480−3483.
(196) Halperin, A.; Zhulina, E. B. On the Deformation Behaviour of Collapsed Polymers. *Eur. Phys. Lett.* **1991**, *15*, 417−420.
(197) Cooke, I. R.; Williams, D. R. M. Stretching Polymers in Poor and Bad Solvents: Pullout Peaks and an Unraveling Transition. *Europhys. Lett.* **2003**, *64*, 267−273.
(198) Li, I. T. S.; Walker, G. C. Signature of Hydrophobic Hydration in a Single Polymer. *Proc. Natl. Acad. Sci. U. S. A.* **2011**, *108*, 16527−16532.
(199) Wu, D.; Lenhardt, J. M.; Black, A. L.; Akhremitchev, B. B.; Craig, S. L. Molecular Stress Relief through a Force-Induced Irreversible Extension in Polymer Contour Length. *J. Am. Chem. Soc.* **2010**, *132*, 15936−15938.
(200) Huang, W.; Zhu, Z.; Wen, J.; Wang, X.; Qin, M.; Cao, Y.; Ma, H.; Wang, W. Single Molecule Study of Force-Induced Rotation of Carbon-Carbon Double Bonds in Polymers. *ACS Nano* **2017**, *11*, 194−203.
(201) Radiom, M.; Kong, P.; Maroni, P.; Schafer, M.; Kilbinger, A. F.; Borkovec, M. Mechanically Induced Cis-to-Trans Isomerization of Carbon-Carbon Double Bonds Using Atomic Force Microscopy. *Phys. Chem. Chem. Phys.* **2016**, *18*, 31202−31210.
(202) Hosono, N.; Kushner, A. M.; Chung, J.; Palmans, A. R.; Guan, Z.; Meijer, E. W. Forced Unfolding of Single-Chain Polymeric Nanoparticles. *J. Am. Chem. Soc.* **2015**, *137*, 6880−6888.
(203) Rakshit, S.; Sivasankar, S. Cross-Linking of a Charged Polysaccharide Using Polyions as Electrostatic Staples. *Soft Matter* **2011**, *7*, 2348−2351.
(204) Gunari, N.; Walker, G. C. Nanomechanical Fingerprints of Individual Blocks of a Diblock Copolymer Chain. *Langmuir* **2008**, *24*, 5197−5201.
(205) Tan, X.; Yu, Y.; Liu, K.; Xu, H.; Liu, D.; Wang, Z.; Zhang, X. Single-Molecule Force Spectroscopy of Selenium-Containing Amphiphilic Block Copolymer: Toward Disassembling the Polymer Micelles. *Langmuir* **2012**, *28*, 9601−9605.
(206) Florin, E. L.; Moy, V. T.; Gaub, H. E. Adhesion Forces between Individual Ligand-Receptor Pairs. *Science* **1994**, *264*, 415−417.

DOI: 10.1021/acs.macromol.7b01459
Macromolecules 2018, 51, 3−24

(207) Liu, N.; Zhang, W. Feeling Inter- or Intramolecular Interactions with the Polymer Chain as Probe: Recent Progress in SMFS Studies on Macromolecular Interactions. *ChemPhysChem* **2012**, *13*, 2238−2256.
(208) Cui, S.; Liu, C.; Zhang, W.; Zhang, X.; Wu, C. Desorption Force Per Polystyrene Segment in Water. *Macromolecules* **2003**, *36*, 3779−3782.
(209) Cui, S.; Liu, C.; Zhang, X. Simple Method to Isolate Single Polymer Chains for the Direct Measurement of the Desorption Force. *Nano Lett.* **2003**, *3*, 245−248.
(210) Scherer, A.; Zhou, C.; Michaelis, J.; Brauchle, C.; Zumbusch, A. Intermolecular Interactions of Polymer Molecules Determined by Single-Molecule Force Spectroscopy. *Macromolecules* **2005**, *38*, 9821−9825.
(211) Liu, K.; Song, Y.; Feng, W.; Liu, N.; Zhang, W.; Zhang, X. Extracting a Single Polyethylene Oxide Chain from a Single Crystal by a Combination of Atomic Force Microscopy Imaging and Single-Molecule Force Spectroscopy: Toward the Investigation of Molecular Interactions in Their Condensed States. *J. Am. Chem. Soc.* **2011**, *133*, 3226−3229.
(212) Song, Y.; Feng, W.; Liu, K.; Yang, P.; Zhang, W.; Zhang, X. Exploring the Folding Pattern of a Polymer Chain in a Single Crystal by Combining Single-Molecule Force Spectroscopy and Steered Molecular Dynamics Simulations. *Langmuir* **2013**, *29*, 3853−3857.
(213) Goodman, D.; Kizhakkedathu, J. N.; Brooks, D. E. Evaluation of an Atomic Force Microscopy Pull-Off Method for Measuring Molecular Weight and Polydispersity of Polymer Brushes: Effect of Grafting Density. *Langmuir* **2004**, *20*, 6238−6245.
(214) Al-Baradi, A.; Tomlinson, M. R.; Zhang, Z. J.; Geoghegan, M. Determination of the Molar Mass of Surface-Grafted Weak Polyelectrolyte Brushes Using Force Spectroscopy. *Polymer* **2015**, *67*, 111−117.
(215) Tischer, T.; Gralla-Koser, R.; Trouillet, V.; Barner, L.; Barner-Kowollik, C.; Lee-Thedieck, C. Direct Mapping of RAFT Controlled Macromolecular Growth on Surfaces Via Single Molecule Force Spectroscopy. *ACS Macro Lett.* **2016**, *5*, 498−503.
(216) Radmacher, M.; Tillmann, R. W.; Gaub, H. E. Imaging Viscoelasticity by Force Modulation with the Atomic Force Microscope. *Biophys. J.* **1993**, *64*, 735−742.
(217) Chizhik, S. A.; Huang, Z.; Gorbunov, V. V.; Myshkin, N. K.; Tsukruk, V. V. Micromechanical Properties of Elastic Polymeric Materials as Probed by Scanning Force Microscopy. *Langmuir* **1998**, *14*, 2606−2609.
(218) Tocha, E.; Schönherr, H.; Vancso, G. J. Quantitative Nanotribology by AFM: A Novel Universal Calibration Platform. *Langmuir* **2006**, *22*, 2340−2350.
(219) Yuya, P. A.; Hurley, D. C.; Turner, J. A. Contact-Resonance Atomic Force Microscopy for Viscoelasticity. *J. Appl. Phys.* **2008**, *104*, 074916.
(220) Young, T. J.; Monclus, M. A.; Burnett, T. L.; Broughton, W. R.; Ogin, S. L.; Smith, P. A. The Use of the Peakforce^{TM} Quantitative Nanomechanical Mapping AFM-Based Method for High-Resolution Young's Modulus Measurement of Polymers. *Meas. Sci. Technol.* **2011**, *22*, 125703.
(221) Wang, D.; Russell, T. P.; Nishi, T.; Nakajima, K. Atomic Force Microscopy Nanomechanics Visualizes Molecular Diffusion and Microstructure at an Interface. *ACS Macro Lett.* **2013**, *2*, 757−760.
(222) Tsukruk, V. V.; Huang, Z.; Chizhik, S. A.; Gorbunov, V. V. Probing of Micromechanical Properties of Compliant Polymeric Materials. *J. Mater. Sci.* **1998**, *33*, 4905−4909.
(223) Tranchida, D.; Piccarolo, S.; Soliman, M. Nanoscale Mechanical Characterization of Polymers by AFM Nanoindentations: Critical Approach to the Elastic Characterization. *Macromolecules* **2006**, *39*, 4547−4556.
(224) Scott, W. W.; Bhushan, B. Use of Phase Imaging in Atomic Force Microscopy for Measurement of Viscoelastic Contrast in Polymer Nanocomposites and Molecularly Thick Lubricant Films. *Ultramicroscopy* **2003**, *97*, 151−169.
(225) Hertz, H. Ueber Die Berührung Fester Elastischer Körper. *J. Reine. Angew. Math.* **1882**, *92*, 156−171.
(226) Johnson, K. L.; Kendall, K.; Roberts, A. D. Surface Energy and the Contact of Elastic Solids. *Proc. R. Soc. London, Ser. A* **1971**, *324*, 301−313.
(227) Derjaguin, B. V.; Muller, V. M.; Toporov, Y. P. Effect of Contact Deformations on the Adhesion of Particles. *J. Colloid Interface Sci.* **1975**, *53*, 314−326.
(228) Chung, P. C.; Green, P. F. The Elastic Mechanical Response of Nanoscale Thin Films of Miscible Polymer/Polymer Blends. *Macromolecules* **2015**, *48*, 3991−3996.
(229) Domke, J.; Radmacher, M. Measuring the Elastic Properties of Thin Polymer Films with the Atomic Force Microscope. *Langmuir* **1998**, *14*, 3320−3325.
(230) Chung, P. C.; Glynos, E.; Green, P. F. The Elastic Mechanical Response of Supported Thin Polymer Films. *Langmuir* **2014**, *30*, 15200−15205.
(231) Chung, P. C.; Glynos, E.; Sakellariou, G.; Green, P. F. Elastic Mechanical Response of Thin Supported Star-Shaped Polymer Films. *ACS Macro Lett.* **2016**, *5*, 439−443.
(232) Xia, W.; Song, J.; Hsu, D. D.; Keten, S. Understanding the Interfacial Mechanical Response of Nanoscale Polymer Thin Films Via Nanoindentation. *Macromolecules* **2016**, *49*, 3810−3817.
(233) Nguyen, H. K.; Fujinami, S.; Nakajima, K. Size-Dependent Elastic Modulus of Ultrathin Polymer Films in Glassy and Rubbery States. *Polymer* **2016**, *105*, 64−71.
(234) Cappella, B.; Kaliappan, S. K. Determination of Thermomechanical Properties of a Model Polymer Blend. *Macromolecules* **2006**, *39*, 9243−9252.
(235) Wang, D.; Fujinami, S.; Liu, H.; Nakajima, K.; Nishi, T. Investigation of Reactive Polymer−Polymer Interface Using Nanomechanical Mapping. *Macromolecules* **2010**, *43*, 5521−5523.
(236) Wang, D.; Liang, X.; Russell, T. P.; Nakajima, K. Visualization and Quantification of the Chemical and Physical Properties at a Diffusion-Induced Interface Using AFM Nanomechanical Mapping. *Macromolecules* **2014**, *47*, 3761−3765.
(237) Wang, D.; Nakajima, K.; Liu, F.; Shi, S.; Russell, T. P. Nanomechanical Imaging of the Diffusion of Fullerene into Conjugated Polymer. *ACS Nano* **2017**, *11*, 8660.
(238) Megevand, B.; Pruvost, S.; Lins, L. C.; Livi, S.; Gérard, J. F.; Duchet-Rumeau, J. Probing Nanomechanical Properties with AFM to Understand the Structure and Behavior of Polymer Blends Compatibilized with Ionic Liquids. *RSC Adv.* **2016**, *6*, 96421−96430.
(239) Niu, Y. F.; Yang, Y.; Gao, S.; Yao, J. W. Mechanical Mapping of the Interphase in Carbon Fiber Reinforced Poly(Ether-Ether-Ketone) Composites Using Peak Force Atomic Force Microscopy: Interphase Shrinkage under Coupled Ultraviolet and Hydro-Thermal Exposure. *Polym. Test.* **2016**, *55*, 257−260.
(240) Qu, M.; Deng, F.; Kalkhoran, S. M.; Gouldstone, A.; Robisson, A.; Van Vliet, K. J. Nanoscale Visualization and Multiscale Mechanical Implications of Bound Rubber Interphases in Rubber−Carbon Black Nanocomposites. *Soft Matter* **2011**, *7*, 1066−1077.
(241) Brune, P. F.; Blackman, G. S.; Diehl, T.; Meth, J. S.; Brill, D.; Tao, Y.; Thornton, J. Direct Measurement of Rubber Interphase Stiffness. *Macromolecules* **2016**, *49*, 4909−4922.
(242) Snétivy, D.; Vancso, G. J. Selective Visualization of Atoms in Extended-Chain Crystals of Oriented Poly(Oxymethylene) by Atomic Force Microscopy. *Macromolecules* **1992**, *25*, 3320−3322.
(243) Magonov, S. N.; Sheiko, S. S.; Deblieck, R. A. C.; Möller, M. Atomic Force Microscopy of Gel-Drawn Ultrahigh Molecular Weight Polyethylene. *Macromolecules* **1993**, *26*, 1380−1386.
(244) Thomas, C.; Seguela, R.; Detrez, F.; Miri, V.; Vanmansart, C. Plastic Deformation of Spherulitic Semi-Crystalline Polymers: An in Situ AFM Study of Polybutene under Tensile Drawing. *Polymer* **2009**, *50*, 3714−3723.
(245) Wang, H. P.; Chum, S. P.; Hiltner, A.; Baer, E. Deformation of Elastomeric Polyolefin Spherulites. *J. Polym. Sci., Part B: Polym. Phys.* **2009**, *47*, 1313−1330.

DOI: 10.1021/acs.macromol.7b01459
Macromolecules 2018, 51, 3−24

(246) Franke, M.; Magerle, R. Locally Auxetic Behavior of Elastomeric Polypropylene on the 100 nm Length Scale. *ACS Nano* **2011**, *5*, 4886−4891.
(247) Oderkerk, J.; de Schaetzen, G.; Goderis, B.; Hellemans, L.; Groeninckx, G. Micromechanical Deformation and Recovery Processes of Nylon-6/Rubber Thermoplastic Vulcanizates as Studied by Atomic Force Microscopy and Transmission Electron Microscopy. *Macromolecules* **2002**, *35*, 6623−6629.
(248) Wang, J. T.; Takshima, S.; Wu, H. C.; Shih, C. C.; Isono, T.; Kakuchi, T.; Satoh, T.; Chen, W. C. Stretchable Conjugated Rod−Coil Poly(3-Hexylthiophene)-block-Poly(Butyl Acrylate) Thin Films for Field Effect Transistor Applications. *Macromolecules* **2017**, *50*, 1442−1452.
(249) Uchida, K.; Mita, K.; Matsuoka, O.; Isaki, T.; Kimura, K.; Onishi, H. The Structure of Uniaxially Stretched Isotactic Polypropylene Sheets: Imaging with Frequency-Modulation Atomic Force Microscopy. *Polymer* **2016**, *82*, 349−355.
(250) Lian, C.; Lin, Z.; Wang, T.; Sun, W.; Liu, X.; Tong, Z. Self-Reinforcement of PNIPAm−Laponite Nanocomposite Gels Investigated by Atom Force Microscopy Nanoindentation. *Macromolecules* **2012**, *45*, 7220−7227.
(251) Liu, H.; Fujinami, S.; Wang, D.; Nakajima, K.; Nishi, T. Nanomechanical Mapping on the Deformed Poly(ε-Caprolactone). *Macromolecules* **2011**, *44*, 1779−1782.
(252) Liu, H.; Chen, N.; Fujinami, S.; Louzguine-Luzgin, D.; Nakajima, K.; Nishi, T. Quantitative Nanomechanical Investigation on Deformation of Poly(Lactic Acid). *Macromolecules* **2012**, *45*, 8770−8779.
(253) Sun, S.; Wang, D.; Russell, T. P.; Zhang, L. Nanomechanical Mapping of a Deformed Elastomer: Visualizing a Self-Reinforcement Mechanism. *ACS Macro Lett.* **2016**, *5*, 839−843.
(254) Morozov, I. A. Structural−Mechanical AFM Study of Surface Defects in Natural Rubber Vulcanizates. *Macromolecules* **2016**, *49*, 5985−5992.
(255) Tsui, O. K. C.; Wang, X. P.; Ho, J. Y. L.; Ng, T. K.; Xiao, X. Studying Surface Glass-to-Rubber Transition Using Atomic Force Microscopic Adhesion Measurements. *Macromolecules* **2000**, *33*, 4198−4204.
(256) Cappella, B.; Kaliappan, S. K.; Sturm, H. Using AFM Force−Distance Curves to Study the Glass-to-Rubber Transition of Amorphous Polymers and Their Elastic−Plastic Properties as a Function of Temperature. *Macromolecules* **2005**, *38*, 1874−1881.
(257) Yablon, D. G.; Gannepalli, A.; Proksch, R.; Killgore, J.; Hurley, D. C.; Grabowski, J.; Tsou, A. H. Quantitative Viscoelastic Mapping of Polyolefin Blends with Contact Resonance Atomic Force Microscopy. *Macromolecules* **2012**, *45*, 4363−4370.
(258) Igarashi, T.; Fujinami, S.; Nishi, T.; Asao, N.; Nakajima, K. Nanorheological Mapping of Rubbers by Atomic Force Microscopy. *Macromolecules* **2013**, *46*, 1916−1922.
(259) An, R.; Huang, L.; Mineart, K. P.; Dong, Y.; Spontak, R. J.; Gubbins, K. E. Adhesion and Friction in Polymer Films on Solid Substrates: Conformal Sites Analysis and Corresponding Surface Measurements. *Soft Matter* **2017**, *13*, 3492−3505.
(260) Braun, O. M.; Naumovets, A. G. Nanotribology Microscopic Mechanisms of Friction. *Surf. Sci. Rep.* **2006**, *60*, 79−158.
(261) Liu, H.; Bhushan, B. Nanotribological Characterization of Molecularly Thick Lubricant Films for Applications to MEMS/NEMS by AFM. *Ultramicroscopy* **2003**, *97*, 321−340.
(262) Drobek, T.; Spencer, N. D. Nanotribology of Surface-Grafted PEG Layers in an Aqueous Environment. *Langmuir* **2008**, *24*, 1484−1488.
(263) Tsukruk, V. V.; Bliznyuk, V. N. Adhesive and Friction Forces between Chemically Modified Silicon and Silicon Nitride Surfaces. *Langmuir* **1998**, *14*, 446−455.
(264) Terada, Y.; Harada, M.; Ikehara, T.; Nishi, T. Nanotribology of Polymer Blends. *J. Appl. Phys.* **2000**, *87*, 2803−2807.
(265) Beake, B. D.; Leggett, G. J.; Shipway, P. H. Nanotribology of Biaxially Oriented Poly(Ethylene Terephthalate) Film. *Polymer* **2001**, *42*, 7025−7031.
(266) Landherr, L. J.; Cohen, C.; Agarwal, P.; Archer, L. A. Interfacial Friction and Adhesion of Polymer Brushes. *Langmuir* **2011**, *27*, 9387−9395.
(267) Dehghani, E. S.; Ramakrishna, S. N.; Spencer, N. D.; Benetti, E. M. Controlled Crosslinking Is a Tool to Precisely Modulate the Nanomechanical and Nanotribological Properties of Polymer Brushes. *Macromolecules* **2017**, *50*, 2932−2941.
(268) Bhairamadgi, N. S.; Pujari, S. P.; Leermakers, F. A.; van Rijn, C. J.; Zuilhof, H. Adhesion and Friction Properties of Polymer Brushes: Fluoro Versus Nonfluoro Polymer Brushes at Varying Thickness. *Langmuir* **2014**, *30*, 2068−2076.
(269) Al-Jaf, O.; Alswieleh, A.; Armes, S. P.; Leggett, G. J. Nanotribological Properties of Nanostructured Poly(Cysteine Methacrylate) Brushes. *Soft Matter* **2017**, *13*, 2075−2084.
(270) Usov, I.; Nystrom, G.; Adamcik, J.; Handschin, S.; Schutz, C.; Fall, A.; Bergstrom, L.; Mezzenga, R. Understanding Nanocellulose Chirality and Structure-Properties Relationship at the Single Fibril Level. *Nat. Commun.* **2015**, *6*, 7564.
(271) Bortolini, C.; Jones, N. C.; Hoffmann, S. V.; Wang, C.; Besenbacher, F.; Dong, M. Mechanical Properties of Amyloid-Like Fibrils Defined by Secondary Structures. *Nanoscale* **2015**, *7*, 7745−7752.
(272) Wang, M.; Jin, H. J.; Kaplan, D. L.; Rutledge, G. C. Mechanical Properties of Electrospun Silk Fibers. *Macromolecules* **2004**, *37*, 6856−6864.
(273) Guo, S.; Akhremitchev, B. B. Packing Density and Structural Heterogeneity of Insulin Amyloid Fibrils Measured by AFM Nanoindentation. *Biomacromolecules* **2006**, *7*, 1630−1636.
(274) Tagit, O.; Tomczak, N.; Vancso, G. J. Probing the Morphology and Nanoscale Mechanics of Single Poly(N-Isopropylacrylamide) Microgels across the Lower-Critical-Solution Temperature by Atomic Force Microscopy. *Small* **2008**, *4*, 119−126.
(275) Rezende, C. A.; Lee, L. T.; Galembeck, F. Surface Mechanical Properties of Thin Polymer Films Investigated by AFM in Pulsed Force Mode. *Langmuir* **2009**, *25*, 9938−9946.
(276) Dietz, C.; Zerson, M.; Riesch, C.; Franke, M.; Magerle, R. Surface Properties of Elastomeric Polypropylenes Studied with Atomic Force Microscopy. *Macromolecules* **2008**, *41*, 9259−9266.
(277) Voss, A.; Stark, R. W.; Dietz, C. Surface Versus Volume Properties on the Nanoscale: Elastomeric Polypropylene. *Macromolecules* **2014**, *47*, 5236−5245.
(278) Tsukruk, V. V.; Sidorenko, A.; Gorbunov, V. V.; Chizhik, S. A. Surface Nanomechanical Properties of Polymer Nanocomposite Layers. *Langmuir* **2001**, *17*, 6715−6719.
(279) Chen, Q.; Schönherr, H.; Vancso, G. J. Mechanical Properties of Block Copolymer Vesicle Membranes by Atomic Force Microscopy. *Soft Matter* **2009**, *5*, 4944−4950.
(280) Lorenzoni, M.; Evangelio, L.; Verhaeghe, S.; Nicolet, C.; Navarro, C.; Perez-Murano, F. Assessing the Local Nanomechanical Properties of Self-Assembled Block Copolymer Thin Films by Peak Force Tapping. *Langmuir* **2015**, *31*, 11630−11638.
(281) Wang, D.; Liang, X. B.; Liu, Y. H.; Fujinami, S.; Nishi, T.; Nakajima, K. Characterization of Surface Viscoelasticity and Energy Dissipation in a Polymer Film by Atomic Force Microscopy. *Macromolecules* **2011**, *44*, 8693−8697.
(282) Dennler, G.; Scharber, M. C.; Brabec, C. J. Polymer-Fullerene Bulk-Heterojunction Solar Cells. *Adv. Mater.* **2009**, *21*, 1323−1338.
(283) Li, G.; Zhu, R.; Yang, Y. Polymer Solar Cells. *Nat. Photonics* **2012**, *6*, 153−161.
(284) Lu, L.; Zheng, T.; Wu, Q.; Schneider, A. M.; Zhao, D.; Yu, L. Recent Advances in Bulk Heterojunction Polymer Solar Cells. *Chem. Rev.* **2015**, *115*, 12666−12731.
(285) Liu, F.; Gu, Y.; Shen, X.; Ferdous, S.; Wang, H. W.; Russell, T. P. Characterization of the Morphology of Solution-Processed Bulk Heterojunction Organic Photovoltaics. *Prog. Polym. Sci.* **2013**, *38*, 1990−2052.
(286) Huang, Y.; Kramer, E. J.; Heeger, A. J.; Bazan, G. C. Bulk Heterojunction Solar Cells: Morphology and Performance Relationships. *Chem. Rev.* **2014**, *114*, 7006−7043.

DOI: 10.1021/acs.macromol.7b01459
Macromolecules 2018, 51, 3−24

(287) Pingree, L. S. C.; Reid, O. G.; Ginger, D. S. Electrical Scanning Probe Microscopy on Active Organic Electronic Devices. *Adv. Mater.* **2009**, *21*, 19−28.
(288) Liscio, A.; Palermo, V.; Samorì, P. Nanoscale Quantitative Measurement of the Potential of Charged Nanostructures by Electrostatic and Kelvin Probe Force Microscopy: Unraveling Electronic Processes in Complex Materials. *Acc. Chem. Res.* **2010**, *43*, 541−550.
(289) Groves, C.; Reid, O. G.; Ginger, D. S. Heterogeneity in Polymer Solar Cells: Local Morphology and Performance in Organic Photovoltaics Studied with Scanning Probe Microscopy. *Acc. Chem. Res.* **2010**, *43*, 612−620.
(290) Musumeci, C.; Liscio, A.; Palermo, V.; Samorì, P. Electronic Characterization of Supramolecular Materials at the Nanoscale by Conductive Atomic Force and Kelvin Probe Force Microscopies. *Mater. Today* **2014**, *17*, 504−517.
(291) Giridharagopal, R.; Cox, P. A.; Ginger, D. S. Functional Scanning Probe Imaging of Nanostructured Solar Energy Materials. *Acc. Chem. Res.* **2016**, *49*, 1769−1776.
(292) Dante, M.; Peet, J.; Nguyen, T. Q. Nanoscale Charge Transport and Internal Structure of Bulk Heterojunction Conjugated Polymer/Fullerene Solar Cells by Scanning Probe Microscopy. *J. Phys. Chem. C* **2008**, *112*, 7241−7249.
(293) Duong, D. T.; Phan, H.; Hanifi, D.; Jo, P. S.; Nguyen, T. Q.; Salleo, A. Direct Observation of Doping Sites in Temperature-Controlled, p-Doped P3HT Thin Films by Conducting Atomic Force Microscopy. *Adv. Mater.* **2014**, *26*, 6069−6073.
(294) Kondo, Y.; Osaka, M.; Benten, H.; Ohkita, H.; Ito, S. Electron Transport Nanostructures of Conjugated Polymer Films Visualized by Conductive Atomic Force Microscopy. *ACS Macro Lett.* **2015**, *4*, 879−885.
(295) Alekseev, A.; Hedley, G. J.; Al-Afeef, A.; Ageev, O. A.; Samuel, I. D. W. Morphology and Local Electrical Properties of PTB7:$PC_{71}BM$ Blends. *J. Mater. Chem. A* **2015**, *3*, 8706−8714.
(296) Osaka, M.; Benten, H.; Ohkita, H.; Ito, S. Intermixed Donor/Acceptor Region in Conjugated Polymer Blends Visualized by Conductive Atomic Force Microscopy. *Macromolecules* **2017**, *50*, 1618−1625.
(297) Osaka, M.; Benten, H.; Lee, L.-T.; Ohkita, H.; Ito, S. Development of Highly Conductive Nanodomains in Poly(3-Hexylthiophene) Films Studied by Conductive Atomic Force Microscopy. *Polymer* **2013**, *54*, 3443−3447.
(298) Wood, D.; Hancox, I.; Jones, T. S.; Wilson, N. R. Quantitative Nanoscale Mapping with Temperature Dependence of the Mechanical and Electrical Properties of Poly(3-Hexylthiophene) by Conductive Atomic Force Microscopy. *J. Phys. Chem. C* **2015**, *119*, 11459−11467.
(299) Reid, O. G.; Munechika, K.; Ginger, D. S. Space Charge Limited Current Measurements on Conjugated Polymer Films Using Conductive Atomic Force Microscopy. *Nano Lett.* **2008**, *8*, 1602−1609.
(300) Bolsée, J. C.; Oosterbaan, W. D.; Lutsen, L.; Vanderzande, D.; Manca, J. CAFM on Conjugated Polymer Nanofibers: Capable of Assessing One Fiber Mobility. *Org. Electron.* **2011**, *12*, 2084−2089.
(301) Moerman, D.; Sebaihi, N.; Kaviyil, S. E.; Leclere, P.; Lazzaroni, R.; Douheret, O. Towards a Unified Description of the Charge Transport Mechanisms in Conductive Atomic Force Microscopy Studies of Semiconducting Polymers. *Nanoscale* **2014**, *6*, 10596−10603.
(302) Coffey, D. C.; Reid, O. G.; Rodovsky, D. B.; Bartholomew, G. P.; Ginger, D. S. Mapping Local Photocurrents in Polymer/Fullerene Solar Cells with Photoconductive Atomic Force Microscopy. *Nano Lett.* **2007**, *7*, 738−744.
(303) Pingree, L. S. C.; Reid, O. G.; Ginger, D. S. Imaging the Evolution of Nanoscale Photocurrent Collection and Transport Networks During Annealing of Polythiophene/Fullerene Solar Cells. *Nano Lett.* **2009**, *9*, 2946−2952.
(304) Hamadani, B. H.; Jung, S.; Haney, P. M.; Richter, L. J.; Zhitenev, N. B. Origin of Nanoscale Variations in Photoresponse of an Organic Solar Cell. *Nano Lett.* **2010**, *10*, 1611−1617.
(305) Xin, H.; Reid, O. G.; Ren, G.; Kim, F. S.; Ginger, D. S.; Jenekhe, S. A. Polymer Nanowire/Fullerene Bulk Heterojunction Solar Cells: How Nanostructure Determines Photovoltaic Properties. *ACS Nano* **2010**, *4*, 1861−1872.
(306) Rice, A. H.; Giridharagopal, R.; Zheng, S. X.; Ohuchi, F. S.; Ginger, D. S.; Luscombe, C. K. Controlling Vertical Morphology within the Active Layer of Organic Photovoltaics Using Poly(3-Hexylthiophene) Nanowires and Phenyl-C_{61}-Butyric Acid Methyl Ester. *ACS Nano* **2011**, *5*, 3132−3140.
(307) Tsoi, W. C.; Nicholson, P. G.; Kim, J. S.; Roy, D.; Burnett, T. L.; Murphy, C. E.; Nelson, J.; Bradley, D. D. C.; Kim, J. S.; Castro, F. A. Surface and Subsurface Morphology of Operating Nanowire: Fullerene Solar Cells Revealed by Photoconductive-AFM. *Energy Environ. Sci.* **2011**, *4*, 3646−3651.
(308) Kamkar, D. A.; Wang, M.; Wudl, F.; Nguyen, T. Q. Single Nanowire OPV Properties of a Fullerene-Capped P3HT Dyad Investigated Using Conductive and Photoconductive AFM. *ACS Nano* **2012**, *6*, 1149−1157.
(309) Hedley, G. J.; Ward, A. J.; Alekseev, A.; Howells, C. T.; Martins, E. R.; Serrano, L. A.; Cooke, G.; Ruseckas, A.; Samuel, I. D. Determining the Optimum Morphology in High-Performance Polymer-Fullerene Organic Photovoltaic Cells. *Nat. Commun.* **2013**, *4*, 2867.
(310) Spadafora, E. J.; Demadrille, R.; Ratier, B.; Grevin, B. Imaging the Carrier Photogeneration in Nanoscale Phase Segregated Organic Heterojunctions by Kelvin Probe Force Microscopy. *Nano Lett.* **2010**, *10*, 3337−3342.
(311) Melitz, W.; Shen, J.; Kummel, A. C.; Lee, S. Kelvin Probe Force Microscopy and Its Application. *Surf. Sci. Rep.* **2011**, *66*, 1−27.
(312) Hoppe, H.; Glatzel, T.; Niggemann, M.; Hinsch, A.; Lux-Steiner, M. C.; Sariciftci, N. S. Kelvin Probe Force Microscopy Study on Conjugated Polymer/Fullerene Bulk Heterojunction Organic Solar Cells. *Nano Lett.* **2005**, *5*, 269−274.
(313) Chiesa, M.; Bürgi, L.; Kim, J. S.; Shikler, R.; Friend, R. H.; Sirringhaus, H. Correlation between Surface Photovoltage and Blend Morphology in Polyfluorene-Based Photodiodes. *Nano Lett.* **2005**, *5*, 559−563.
(314) Baghgar, M.; Barnes, M. D. Work Function Modification in P3HT H/J Aggregate Nanostructures Revealed by Kelvin Probe Force Microscopy and Photoluminescence Imaging. *ACS Nano* **2015**, *9*, 7105−7112.
(315) McFarland, F. M.; Brickson, B.; Guo, S. Layered Poly(3-Hexylthiophene) Nanowhiskers Studied by Atomic Force Microscopy and Kelvin Probe Force Microscopy. *Macromolecules* **2015**, *48*, 3049−3056.
(316) Shao, G.; Glaz, M. S.; Ma, F.; Ju, H.; Ginger, D. S. Intensity-Modulated Scanning Kelvin Probe Microscopy for Probing Recombination in Organic Photovoltaics. *ACS Nano* **2014**, *8*, 10799−10807.
(317) Hamadani, B. H.; Gergel-Hackett, N.; Haney, P. M.; Zhitenev, N. B. Imaging of Nanoscale Charge Transport in Bulk Heterojunction Solar Cells. *J. Appl. Phys.* **2011**, *109*, 124501.
(318) Garcia, R.; Proksch, R. Nanomechanical Mapping of Soft Matter by Bimodal Force Microscopy. *Eur. Polym. J.* **2013**, *49*, 1897−1906.
(319) Rüttiger, C.; Appold, M.; Didzoleit, H.; Eils, A.; Dietz, C.; Stark, R. W.; Stühn, B.; Gallei, M. Structure Formation of Metallopolymer-Grafted Block Copolymers. *Macromolecules* **2016**, *49*, 3415−3426.
(320) Dazzi, A.; Prater, C. B.; Hu, Q.; Chase, D. B.; Rabolt, J. F.; Marcott, C. AFM−IR: Combining Atomic Force Microscopy and Infrared Spectroscopy for Nanoscale Chemical Characterization. *Appl. Spectrosc.* **2012**, *66*, 1365−1384.
(321) Felts, J. R.; Cho, H.; Yu, M. F.; Bergman, L. A.; Vakakis, A. F.; King, W. P. Atomic Force Microscope Infrared Spectroscopy on 15 nm Scale Polymer Nanostructures. *Rev. Sci. Instrum.* **2013**, *84*, 023709.
(322) Gong, L.; Chase, D. B.; Noda, I.; Liu, J.; Martin, D. C.; Ni, C.; Rabolt, J. F. Discovery of β-Form Crystal Structure in Electrospun Poly[(R)-3-Hydroxybutyrate-co-(R)-3-Hydroxyhexanoate] (PHBHx)

DOI: 10.1021/acs.macromol.7b01459
Macromolecules 2018, 51, 3−24

Nanofibers: From Fiber Mats to Single Fibers. *Macromolecules* **2015**, *48*, 6197−6205.
(323) Tang, F.; Bao, P.; Su, Z. Analysis of Nanodomain Composition in High-Impact Polypropylene by Atomic Force Microscopy-Infrared. *Anal. Chem.* **2016**, *88*, 4926−4930.
(324) Felts, J. R.; Kjoller, K.; Lo, M.; Prater, C. B.; King, W. P. Nanometer-Scale Infrared Spectroscopy of Heterogeneous Polymer Nanostructures Fabricated by Tip-Based Nanofabrication. *ACS Nano* **2012**, *6*, 8015−8021.
(325) Shaykhutdinov, T.; Pop, S. D.; Furchner, A.; Hinrichs, K. Supramolecular Orientation in Anisotropic Assemblies by Infrared Nanopolarimetry. *ACS Macro Lett.* **2017**, *6*, 598−602.
(326) Tai, T.; Karacsony, O.; Bocharova, V.; Van Berkel, G. J.; Kertesz, V. Topographical and Chemical Imaging of a Phase Separated Polymer Using a Combined Atomic Force Microscopy/Infrared Spectroscopy/Mass Spectrometry Platform. *Anal. Chem.* **2016**, *88*, 2864−2870.
(327) Hoffmann, W. D.; Kertesz, V.; Srijanto, B. R.; Van Berkel, G. J. Atomic Force Microscopy Thermally-Assisted Microsampling with Atmospheric Pressure Temperature Ramped Thermal Desorption/Ionization-Mass Spectrometry Analysis. *Anal. Chem.* **2017**, *89*, 3036−3042.
(328) Knittel, P.; Mizaikoff, B.; Kranz, C. Simultaneous Nanomechanical and Electrochemical Mapping: Combining Peak Force Tapping Atomic Force Microscopy with Scanning Electrochemical Microscopy. *Anal. Chem.* **2016**, *88*, 6174−6178.
(329) Kodera, N.; Yamamoto, D.; Ishikawa, R.; Ando, T. Video Imaging of Walking Myosin V by High-Speed Atomic Force Microscopy. *Nature* **2010**, *468*, 72−76.
(330) Song, J.; Tranchida, D.; Vancso, G. J. Contact Mechanics of UV/Ozone-Treated PDMS by AFM and JKR Testing: Mechanical Performance from Nano- to Micrometer Length Scales. *Macromolecules* **2008**, *41*, 6757−6762.
(331) Rico, F.; Roca-Cusachs, P.; Gavara, N.; Farre, R.; Rotger, M.; Navajas, D. Probing Mechanical Properties of Living Cells by Atomic Force Microscopy with Blunted Pyramidal Cantilever Tips. *Phys. Rev. E* **2005**, *72*, 021914.

DOI: 10.1021/acs.macromol.7b01459
Macromolecules 2018, 51, 3−24